（千葉大学審査学位論文）

Study of Filter Topologies Using One-Port SAW/BAW Resonators and Lumped Circuit Elements

(1 ポート SAW / BAW 共振子と集中定数要素を組み合わせたフィルタ構成に関する研究）

2018 年 7 月

千葉大学大学院工学研究科
人工システム科学専攻電気電子系コース

黄 裕霖

Ph.D. thesis submitted in partial fulfillment of the requirements for the degree of Ph.D. in Science, Graduate School of Chiba University, Japan.

Affiliation:

Graduate School of Engineering

Department of Electrical and Electronic Engineering

Chiba University

1-33 Yayoi-cho, Inage-ku, Chiba-shi 263-8522 Japan

Supervisor:

Prof. Ken-ya Hashimoto, Dep. Elec. and Electronic Engineering, Graduate School of Engineering, Chiba University

Examiners:

Prof. Ken-ya Hashimoto, Dep. Elec. and Electronic Engineering, Graduate School of Engineering, Chiba University

Prof. Toshiaki Takano, Dep. Elec. and Electronic Engineering, Graduate School of Engineering, Chiba University

Prof. Kazuhiro Kudo, Dep. Elec. and Electronic Engineering, Graduate School of Engineering, Chiba University

Prof. Tatsuya Omori, Dep. Elec. and Electronic Engineering, Graduate School of Engineering, Chiba University

DECLARATION

I hereby declare that this submission is my own work and that, to the best of my knowledge and belief, it contains no material which to a substantial extent has been accepted for the award of any other degree or diploma of the university or other institute of higher learning, except where due acknowledgement has been made in the text.

Yulin Huang, Chiba, July 2018

ACKNOWLEDGEMENT

This thesis was prepared during my stay in the Electro-Communications Laboratory of Chiba University, Japan.

First, I want to thank my supervisor, Prof. Ken-ya Hashimoto, for his detailed instructions and patient guidance during my three years study in Chiba University. It’s my great honor to be a student of Prof. Hashimoto who is a very brilliant and energetic man. He leads me into acoustic field from electronic field step by step, advise my research conscientiously, and offers me lots of good opportunities on symposiums and enterprises. He is very strict on study and research while very kind hearted on daily life. I learned quite a lot from him not only on acoustic field but also on the attitude to people and life.

I am also grateful for Prof. Jingfu Bao from University of Electronic Science and Technology of China (UESTC), who provided me the chance to be involved in this double Ph.D. degree program between UESTC and Chiba University. He instructed me on electronic field for many years and offers me many opportunities including this double degree program to extend my vision.

The efforts for reviewing the dissertation by Prof. Toshiaki Takano, Prof. Kazuhiro Kudo, Prof. Tatsuya Omori are appreciated. I also want to express gratitude to Prof. Tatsuya Omori for offers me instructions in using almost all the instruments.

Thanks should also be given to all the members of the Electro-Communications Laboratory of Chiba University. For the good time I have enjoyed, I would like to express my gratitude for all the students with whom I have shared the office, they are Gongbin Tang, Benfeng Zhang, Qiaozhen Zhang, Xinyi Li and Luyan Qiu. Thanks for the help from them and their families on my study and life.

I am also grateful to the IEEE and the JJAP for their devotion to the promotion of research by providing platforms for scientific publications, organizing scientific conferences and their financial support to students.

At Last, I wish to thank all of my family members for their great understanding, support and suffering of separation in these years. To them I dedicate this thesis.

ABSTRACT

This thesis aims to obtain high performance, small size and low cost SAW/BAW filters. To achieve this, several problems from traditional SAW/BAW filters are solved by applying special designed topological structures where one–port SAW/BAW resonators are combined with lumped circuit elements.

First, SAW-BAW-based band reject filter composed of the impedance converters is studied. Basic properties of the unit cell are studied including pass band and reject band. It also shows that when two notches caused by the resonators are placed in proximity, two synergy effects occur and the filter performance enhanced. Then, two resonators are fabricated, measured and combined with inductors in circuit simulator to demonstrate functionality of the basic cell design. Finally, the wide rejection band filter is designed by cascading multi-stages, and effectiveness of the device configurations is demonstrated.

Then, possibility is discussed to realize multimode filters composed of multiple single-mode resonators by using radio frequency surface and bulk acoustic wave (SAW/BAW) technologies. The filter operation and design principle are given. Excellent filter characteristics have been achieved by combining multiple one-port resonators with identical capacitance ratios. Next, the effect of balun performance is investigated. It is shown that the total filter performance is significantly degraded by balun imperfections such as the common-mode rejection. At last, two circuits are proposed to improve the common-mode rejection, and their effectiveness are demonstrated.

LIST OF CONTENTS

Introduction

1.1 Background

Acoustic devices are fabricated on piezoelectric materials such like quartz, $LiTaO_3$, $LiNbO_3$ etc., and are recognized as one of the key elements in communication systems. Piezoelectricity is the ability of materials with crystallographic asymmetry to generate electric charges in response to applied mechanical stress. Since the propagation speed of acoustic wave is 5 orders smaller than the electromagnetic wave, the size of acoustic devices can be much smaller than traditional electromagnetic ones. From this advantage, SAW devices have been widely used in military radar, electromagnetic countermeasure and commercial wireless communication systems.

Acoustic waves include the surface and the bulk acoustic waves (SAW/BAW). SAW was firstly derived theoretically by Lord Rayleigh in 1885 [1.1] as an acoustic wave with energy concentration in the depth smaller than one wavelength from the surface. The typical structure of SAW resonators is shown in Figure 1.1. It contains an interdigital transducers (IDT) and grating reflectors on the piezoelectric substrate. SAW resonances between the grating reflectors are excited and detected electrically by the IDT. Use of IDTs for SAW excitation was firstly proposed by R. M. White and F. M. Voltmer in 1965 [1.2]. Because the electrode and grating film thicknesses is usually uniform, SAW fabrication process is relatively simple. Nevertheless, tight control of the film thickness and properties is mandatory in addition to fine patterning of these electrodes.

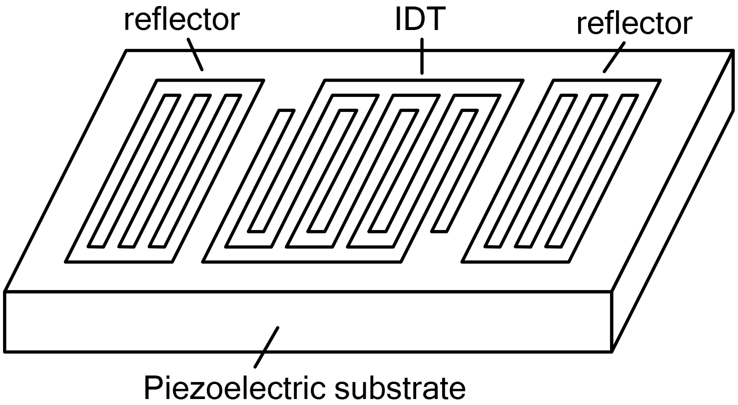

Figure 1.1 Typical structure of SAW resonator

BAW, which propagates in the bulk instead of the surface, is also widely used as acoustic resonators. The BAW resonators can be categorized to two types: the film bulk acoustic resonator (FBAR) [1.3][1.4] and solidly mounted resonators (SMR) [1.5]~[1.7] as shown in Figure 1.2. FBAR isolates the piezoelectric layer from the substrate acoustically by the air cavity while SMR employs the Bragg reflector. Acoustic resonances occur mainly between two electrodes, and are excited by electric fields between them.

The lateral size of the electrodes is much larger than the wavelength determined by the thickness of piezoelectric layer. Since BAW energy is confined in this layer and it is isolated acoustically from the supporting substrate, BAW resonators are believed to offer better quality factor *Q* than SAW resonators. Furthermore, BAW devices offer better durability against radio frequency (RF) signal power. This is because the acoustic-migration limiting life time of SAW devices hardly occurs in BAW devices.

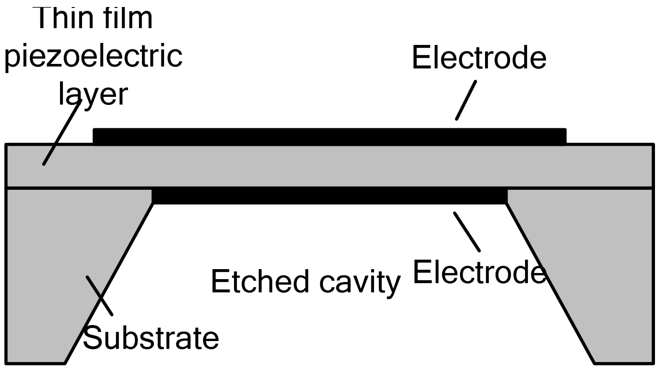

(a)

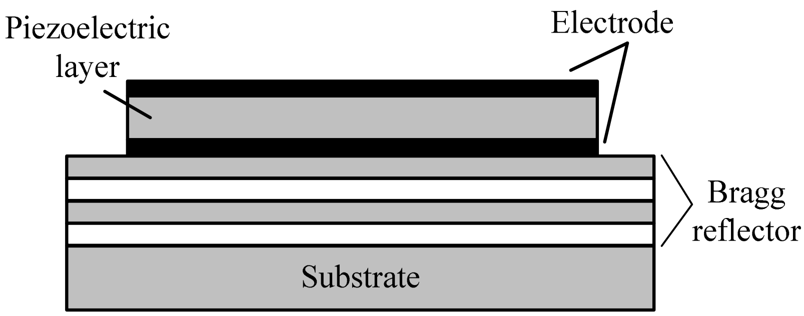

(b)

Figure 1.2 Typical structure of BAW resonator for (a) FBAR and (b) SMR

Presently, main application of SAW/BAW resonators is filters for frequency selection in the RF range. They play very important roles in wireless communications. Representative is RF frontend filters and duplexers in mobile and smart phones. In addition to their vast number of annual sales, introduction of new frequency bands and standards expands the market size of SAW/BAW resonators explosively. Nowadays, there are more than 40 LTE (long time evolution) bands. In the market, SAW devices are dominant for the frequency bands under 1 GHz while SAW and BAW devices have their own shares above 1 GHz [1.3][1.8][1.9].

Usually SAW/BAW filters offer band pass characteristics. Figure 1.3 shows the filter configuration called the ladder-type [1.10]. The basic concept is to set the anti-resonance frequency of the parallel resonators equal to the resonance frequency of the series resonators. Then almost 100% signal transfer is possible between the input and output ports at this frequency. At frequencies far from these resonances, since resonators can be regarded as simple capacitors, cascading multiple sections allows us to enhance suppression of the signal transfer. Note that the resonance of the parallel resonators and the anti-resonance of the series resonators create transmission zeros. Then a flat passband sandwiched in between two zeros appears. This filter topology offers low insertion loss in the passband and high durability against RF input power [1.11]~[1.14]. From these features, this topology is widely used in duplexers which will be described later. One drawback is inferior out of band rejection.

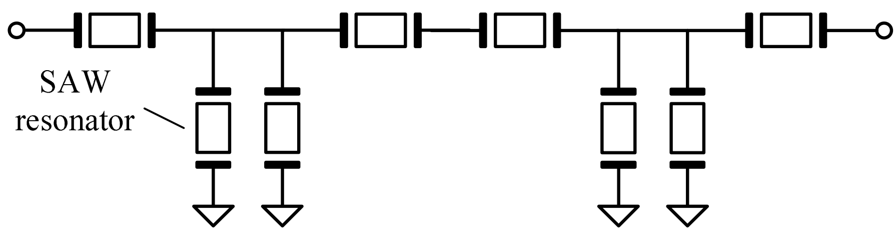

Figure 1.3 Structure of ladder-type filter

The lattice filter configuration is another choice [1.15]~[1.17]. However, its applicability is limited because it is only applicable to cases with balanced input and output.

Duplexers are three port devices realized by parallel connecting input ports of two filters with different passbands, one is called the receive (Rx) band for the signal transmission from the antenna to the hand set, and another one is call the transmit (Tx) band for the signal transmission from the hand set to the antenna. Parallel connected port is called the antenna (ANT) port while remaining two are called the Tx and Rx ports. Duplexer, antenna and amplifiers formed the RF front-end as shown in Figure 1.4. The most important function of the duplexer is to suppress signal transfer between the Tx and Rx ports, and the suppression level called isolation is highly demanded to be enhanced to 70 dB. For efficient use of frequency resources, the frequency gap between Tx and Rx bands is going to be extremely narrow. For example, the fractional gap width in Band 25 is only 0.75%.

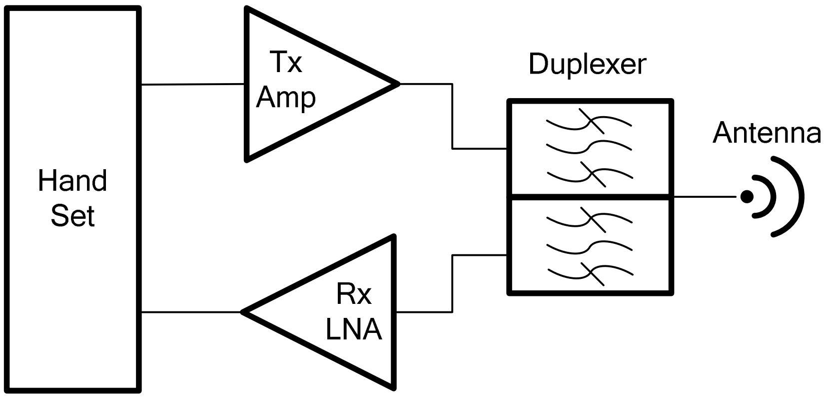

Figure 1.4 Structure of RF front-end

Since SAW/BAW duplexers are used in the RF frontend of transceivers, ultimate loss reduction is requested in the Rx band not to deteriorate detection sensitivity. Furthermore, it is also requested for the Tx band so as to reduce the battery power consumption and self-heating [1.18]. So as to fulfill these tight requirements, inclusion of the band reject function is paid much attention in SAW/BAW filters and duplexers. For example, the function may be able to enhance the isolation without scarcely deteriorating the passband characteristics [1.19][1.20].

SAW notch filters can be composed by embedding SAW resonators in all pass filters [1.21]~[1.23]. C.S.Hartmann, et al, proposed to use twin-peak IDTs for expanding the rejection bandwidth [1.24]. In 1990, S.Gompani, et al. proposed a notch filter using a two-pole waveguide coupled resonator embedded in an all pass network [1.25]. Expansion of the rejection bandwidth was also discussed in [1.26] where multiple SAW resonators are series connected.

Another type of SAW filters called the double mode SAW (DMS) filters [1.27] is also widely used. Figure 1.5 shows its basic configuration, the structure is designed so as to support multiple resonances, and proper arrangement of these resonances enables us to synthesize the flat passband and sharp cutoff characteristics [1.28]. Far from the resonances, signal transfer between two IDTs is weak, and thus good out-of-band rejection can be achievable [1.28]~[1.31]. However, DMS filters exhibit higher insertion loss than ladder-type SAW filters. Furthermore, DMS filters have much worse power durability than the ladder-type. In recent duplexers, it is common to use ladder-type and DMS filters for Tx and Rx bands, respectively.

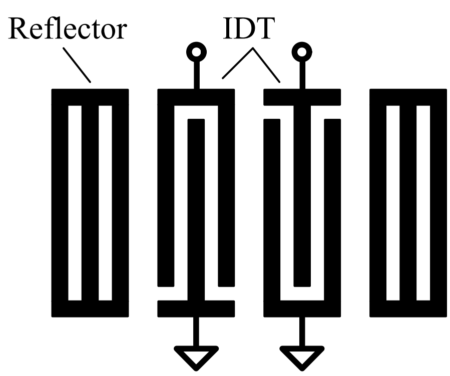

Figure 1.5 Structure of DMS filter

The ladder type configuration is widely used also for BAW devices. Acoustically coupled BAW resonator filters are investigated extensively to realize excellent out-of-band rejection like DMS filters. Figure 1.6 shows an example called coupled-resonator-filter (CRF) [1.32]~[1.35]. Two BAW resonators are stacked and their acoustic coupling is adjusted by the sandwiched center layer. Its operation principle is the same as that of the DMS filter, and flat passband and good out-of-band rejection can be achieved simultaneously by properly designing the coupling layer.

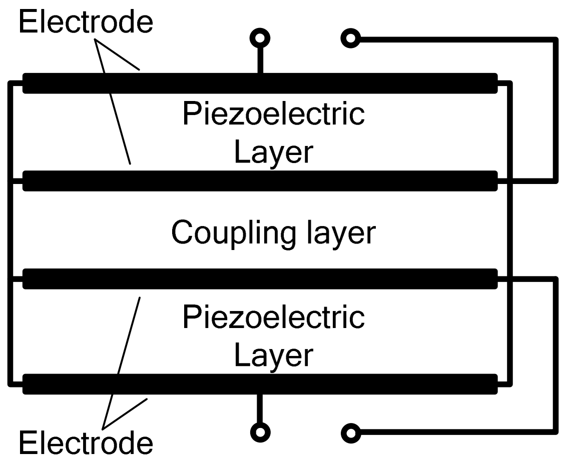

Figure 1.6 Structure of coupled resonator filter

Although excellent performances were reported [1.35], CRFs are never mass produced. This is because tricky mechanisms and materials are needed for weakening the coupling, and their process control is extremely difficult.

1.2 Motivation

To enhance performance of SAW/BAW filters further, the following problems should be solved.

1) SAW/BAW band reject filters are paid much interested, and many devices with

excellent performance are published. However, their design procedures have never been discussed in detail.

2) DMS filters offer excellent out of band rejection but inferior power durability. Although CRFs offer both good out-of-band rejection and good power durability, their mass production is difficult.

1.3 Purpose

To solve the problems listed above, this thesis studied the following topics.

1). A band reject filter embedded in impedance converter is studied to verify the possibility of impedance converter combination and discuss the design procedure in detail.

2). A multi-mode filter is proposed based on electrical coupling to support both SAW and BAW resonators and its differential structure will ensure the excellent out of band attenuation.

1.4 Organization of this thesis

Chapter 2 studied the SAW-BAW-based band reject filter composed of the impedance converters. Basic properties of the unit cell are studied including pass band and reject band. It also shows that when two notches caused by the resonators are placed in proximity, two synergy effects occur and the filter performance enhanced. Then, two resonators are fabricated, measured and combined with inductors in circuit simulator to demonstrate functionality of the basic cell design. Finally, the wide rejection band filter is designed by cascading multi-stages, and effectiveness of the device configurations is demonstrated.

Chapter 3 discussed the possibility of realizing multimode filters composed of multiple single-mode resonators by using radio frequency surface and bulk acoustic wave (SAW/BAW) technologies. The filter operation and design principle are given. It is shown that excellent filter characteristics are achievable by combining multiple single-mode resonators with identical capacitance ratios provided that their resonance frequencies and clamped capacitances are set properly. Next, the effect of balun performance is investigated. It is shown that the total filter performance is significantly degraded by balun imperfections such as the common-mode rejection. Then, two circuits are proposed to improve the common-mode rejection, and their effectiveness is demonstrated.

Chapter 4 draws the conclusion of the whole thesis.

Reference

[1.1] L. Rayleigh, “On waves propagated along the plane surface of elastic solid,” *Proc. London Math. Society* 17 (1885) p. 4.

[1.2] R. M. White, and F. W. Voltmer, “Direct piezoelectric coupling to surface elastic waves,” *Appl. Phys. Lett.* 7 (1965) p. 314.

[1.3] R. Ruby, M. Small, F. Bi, D. Lee, L. Callaghan, R. Parker, and S. Ortiz, "Positioning FBAR technology in the frequency and timing domain," *IEEE Trans.*

Ultrasonics Ferroelectr. Freq. Control 59 (2012) p. 334.

[1.4] R. Ruby, P. Bradley, Y. Oshmyansky, and A. Chien, "Thin film bulk wave acoustic resonators (FBAR) for wireless applications," *Proc. IEEE Ultrason. Symp.* (2001) p. 813.

[1.5] K. M. Lakin, K. T. McCarron, and R. E. Rose, "Solidly mounted resonators and filters," *Proc. IEEE Ultrasonics Symp.* (1995) p. 905.

[1.6] H. Kanbara, H. Kobayashi, and K. Nakamura, "Analysis of piezoelectric thin film resonators with acoustic quarter-wave multilayers," *Jpn. J. Appl. Phys.* 39 (2000) p. 3049

[1.7] H. Kobayashi, Y. Ishida, K. Ishikawa, A. Doi, and K. Nakamura, "Fabrication of piezoelectric thin film resonators with acoustic quarter-wave multilayers," *Jpn. J. Appl. Phys.* 41 (2002) p. 3455.

[1.8] A. Suzuki, K. Ueda, S. Goka, K. Wada, and S. Kakio, "Multiplex transmission system for gate drive signals of inverter circuit using surface acoustic wave filters," *Jpn. J. Appl. Phys.* 55 (2016) 07KD01.

[1.9] M. Kadota and S. Tanaka, "Ultra-wideband ladder filters using zero-th shear mode plate wave in ultrathin $LiNbO_3$ plate with apodized interdigital transducers," *Jpn. J. Appl. Phys.* 55 (2016) 07KD04

[1.10] R. A. Sykes, "A new approach to the design of high frequency crystal filters," *IRE National Convention* (1958) p. 18.

[1.11] S. C.-C. Tseng and G. W. Lynch, "SAW planar network," *Proc. IEEE Ultrason.*

Symp. (1974) p. 282.

[1.12] M. Kadota, & S. Tanaka, "Ultra-wideband ladder filter using SH 0 plate wave in thin LiNbO3 plate and its application to tunable filter", *IEEE Trans. Ultrasonics Ferroelectr. Freq. Control,* 62 (2015) p. 939.

[1.13] K. Y. Hashimoto, T. Kimura, T. Matsumura, H. Hirano, M. Kadota, M. Esashi, M., & S. Tanaka, "Moving Tunable Filters Forward". *IEEE Microwave Magazine,* 16 (2015) p. 89.

[1.14] T. Takai, H. Iwamoto, Y. Takamine, T. Fuyutsume, T. Nakao, M. Hiramoto, ... & M. Koshino, "IHP SAW technology and its application to microacoustic components," *Proc. IEEE Ultrason. Symp.* (2017) DOI: 10.1109/ULTSYM.2017.8091876

[1.15] J. Heighway, S. N. Kondratiev, and V. P. Plessky, "Balanced Bridge SAW Impedance Element Filters," *Proc. IEEE Ultrason. Symp.* (1994) p. 27

[1.16] M. A. Dubois, J. F. Carpentier, P. Vincent, C. Billard, G. Parat, C. Muller, P. Ancey, and P. Conti, "Monolithic above-IC resonator technology for integrated architectures in mobile and wireless communication", *IEEE Journal of Solid State Circuits,* 41 (2006) p. 7

[1.17] Q. Yang, W. Pang, D. Zhang, and H. Zhang, "A Modified Lattice Configuration Design for Compact Wideband Bulk Acoustic Wave Filter Applications," *Micromachines*, 7 (2016) p. 133

[1.18] T. Bauer, C. Eggs, K. Wagner, and P. Hagn, "A bright outlook for acoustic filtering: A new generation of very low-profile SAW, TC SAW, and BAW devices for module integration," *IEEE Microwave Magazine,* 16 (2015) p. 73.

[1.19] V. Gozhenko, W. Puffer, D. Ritter, and A. Przadka, "High Performance WCDMA1900 Combined LTCC/SAW/BAW Duplexer for Mobile Phones," *European Microwave Conf.* (2008) p. 618

[1.20] T. Nishihara, M. Iwaki, G. Endo, X. Mi, S. Taniguchi, M. Ueda, Y. Satoh, "BAW/SAW/IPD hybrid type duplexer with Rx balanced output for WCDMA Band I," *Tech. Digest, IEEE Microwave Conf.* (2008) p. 831

[1.21] Y. Koyamada, F. Ishihara, and Y. Yoshikawa, "Band Elimination Filter Employing Surface Acoustic Wave Resonator", *Electronics, Letters,* 11, 5 (1975) p. 108

[1.22] D. P. Akiit, "70 MHz Surface-Acoustic-Wave Resonator Notch Filter," *Electronics Letters,* 12, 9 (1976) p. 217

[1.23] M. Lewis and C. L. West, "Use of acoustic transducers as generalized electrical circuit elements," *Electronics Letters,* 21, 25 (1985) p. 1211

[1.24] C. S. Hartmann, J. C. Andle and M.B. King, "SAW Notch Filters," *Proc. IEEE Ultrason. Symp.* (1987) p. 131

[1.25] S. Gopani and B. A. Horine, "SAW Waveguide Coupled Resonator Notch Filter," *Proc. IEEE Ultraso. Symp.* (1990) p. 1

[1.26] P. V. Wright, "A new generalized modeling of SAW transducers and gratings," *Proc. IEEE Freq. Contr. Symp.* (1989) p. 595

[1.27] T. Morita, Y. Watanabe, M. Tanaka, & Y. Nakazawa, “Wideband low loss double mode SAW filters,” *Proc. IEEE Ultrason. Symp.* (1992) p. 95.

[1.28] K. Hashimoto, T. Omori, and M. Yamaguchi, “Operation mechanism of double-mode surface acoustic wave filters with pitch-modulated IDTs and reflectors,” *IEEE Trans. Ultrason. Ferroelectr. Freq. Control,* 54 (2007) p. 2152

[1.29] M. Kadota, “Development of substrate structures and processes for practical applications of various surface acoustic wave devices,” *Jpn. J. Appl. Phys.* 44 (2005) p. 4285.

[1.30] V. Gozhenko, W. Puffer, D. Ritter, and A. Przadka, “High Performance WCDMA1900 Combined LTCC/SAW/BAW Duplexer for Mobile Phones,” *European Microwave Conf.* (2008) p. 618.

[1.31] T. Nishihara, M. Iwaki, G. Endo, X. Mi, S. Taniguchi, M. Ueda, and Y. Satoh, “BAW/SAW/IPD Hybrid Type Duplexer with Rx Balanced Output for WCDMA Band I,” *Tech. Dig., IEEE Microwave Conf.* (2008) p. 831.

[1.32] K. M. Lakin, “Coupled Resonator Filters,” *Proc. IEEE Ultrason. Symp,* 1 (2002) p. 901.

[1.33] G. Fattinger, R. Aigner, & W. Nessler, “Coupled Bulk Acoustic Wave Resonator Filter: Key Technology for Single-to-Balanced RF Filters,” *Proceedings IEEE 2004 MTS Symp. Digest,* 2 (2004) p. 927.

[1.34] K. M. Lakin, Proc. "Bulk acoustic wave coupled resonator filters," *IEEE Frequency Control Symp,* (2002) p. 8.

[1.35] G. G. Fattinger, J. Kaitila, R. Aigner, and W. Nessler, "Single-to-balanced filters for mobile phones using coupled resonator BAW technology," *Proc. IEEE Ultrasonics Symp.* (2004) p. 416.

2 Band reject filters using SAW/BAW resonators embedded into impedance converter

2.1 Introduction

Impedance converters are quite often used in RF circuits and modules such as the output stage of power amplifiers [2.1]. Thus use of SAW/BAW resonators may embed the band reject function into RF modules in order to decrease the complexity of circuit and further minimize the device size. Furthermore, since inductors are also quite often used for impedance matching in RF circuits including SAW/BAW filters and duplexers, they may be also used for the same purpose.

This chapter describes a filter based on ladder like structures and the filter both has the band stop function and impedance convert function.

After a brief introduction of traditional ladder type filter design, the basic properties of the unit cell including pass band and reject band are discussed. It is shown that when two notches are placed in proximity, two synergy effects occur: (i) an extra matching point appears on one side of the transition band. This make the insertion loss at the point smaller and the transition band steeper, and (ii) the dip level becomes deeper, and the total rejection level becomes better.

Then, functionality of the basic cell design is demonstrated using two SAW resonators fabricated on 42-LT. The filter operation is examined on a circuit simulator in combination with built-in inductors.

Finally, the wide rejection band filter is designed by cascading multi-stages, and effectiveness of the proposed design procedure is examined.

2.2 Design principle of traditional ladder-type filter

The idea of designing traditional ladder-type bandpass filter is utilizing the poles from acoustic resonators to create low loss signal path. Figure 2.1 shows the typical topology of a ladder-type filter, which applies SAW/BAW resonator R_1 on the serial arm and R_2 on the parallel arm.

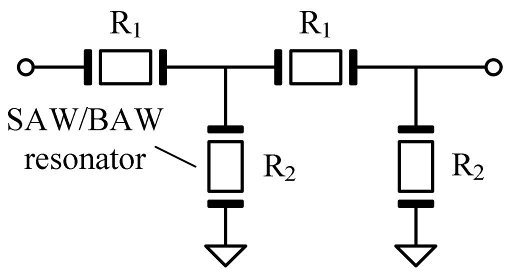

Figure 2.1 Ladder type bandpass filter topological structure

Figure 2.2 shows the characteristics of the filter comparing with its resonators impedance. In the figure, f_{pr} and f_{pa} represent the resonance and anti-resonance frequency of R_1, f_{sr} and f_{sa} represent the ones of R_2. In the passband, the serial resonator should work near f_{sr} to obtain impedance close to zero, while the parallel resonator should work near f_{pa} for very high impedance. So that the serial path is close to short circuited and parallel path is close to open circuited, and low loss transmission is achieved. With the single mode acoustic resonator, the resonance frequency always appears lower than the anti-resonance frequency. Then f_{sr} should be larger than f_{pa} in order to have a flat passband. There are two deep notches just below and above the passband. The one below the passband is caused by the small parallel impedance on f_{pr}, which makes most of the signal been absorbed by ground. The one above the passband is caused by the large serial impedance on f_{sa}, which reflected most of the signal back to source. Far away from the passband, the acoustic resonator act as capacitors and the out-of-band attenuation becomes bad.

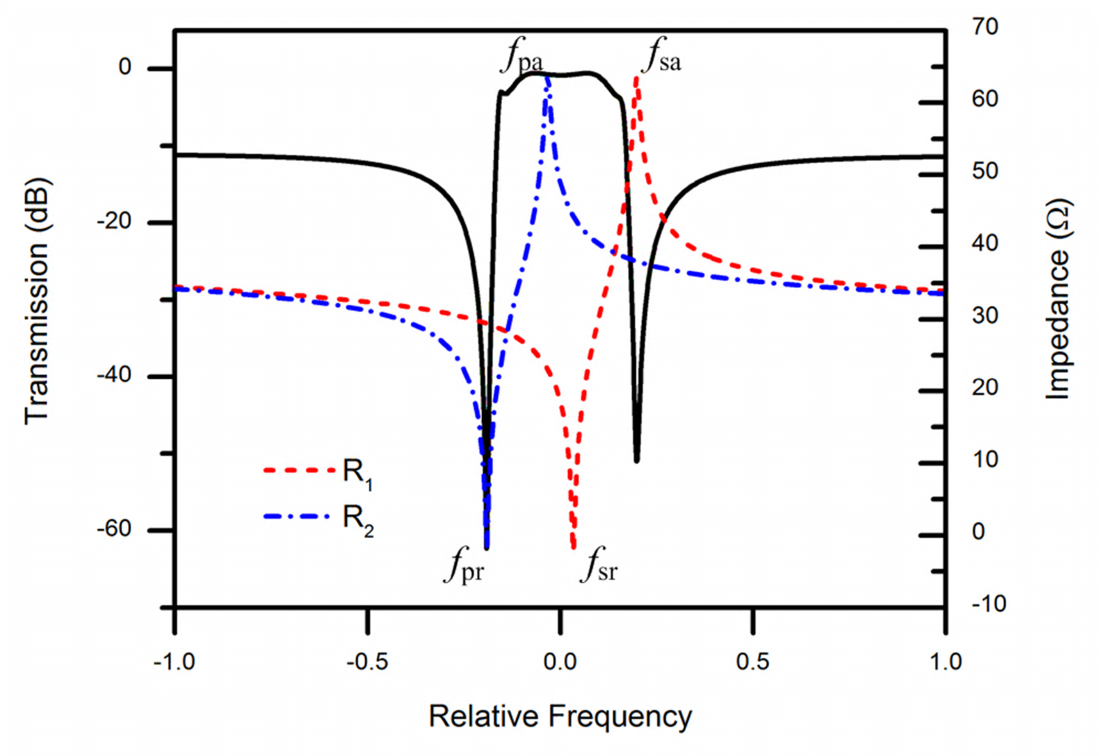

Figure 2.2 Ladder type bandpass filter characteristics variating with the serial and parallel arm impedance

2.3 Consideration on basic cells of band reject filter

Similar to the filter described above, this band reject filter applies ladder-like topological structure. However, its transmission function is opposite to the band pass filter and requires different settings such like the resonator notch positions and additional inductive elements.

2.3.1 L-matching network

L-matching network is a well-known two port network combined of one serial impedance and one parallel impedance as shown in Figure 2.3, where Z_s and Z_p are the impedance of serial arm and parallel arm, Z_1 and Z_2 are the smaller and larger input impedance of two ports, respectively. Due to its asymmetric nature, its input impedance of two ports should be different when the whole structure is well matched. Thus, the L-matching network is usually used as the impedance converter.

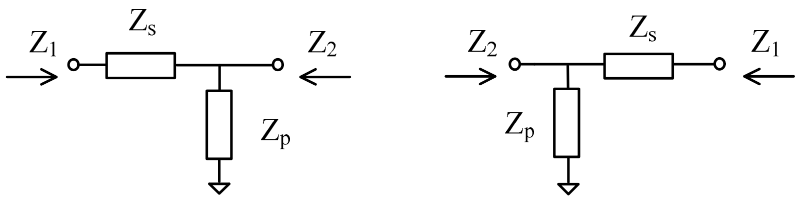

(a) Step up (Z_2>Z_1) (b) Step down (Z_1<Z_2)

Figure 2.3 Impedance converters (L-matching network)

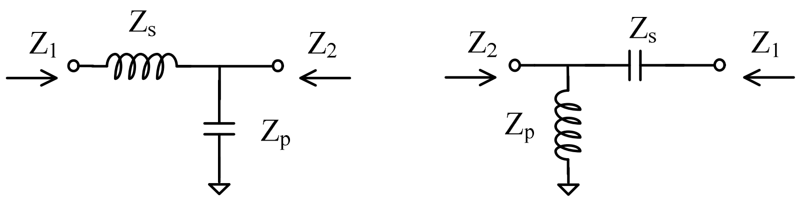

(a) Step up (Z_2>Z_1) (b) Step down (Z_1<Z_2)

Figure 2.4 L-matching network with lumped elements

Z_s and Z_p are usually set to be pure imaginary for lossless signal transmission. For lumped element case, the pure imaginary impedance could be realized by replacing two arms with capacitors and inductors as shown in Figure 2.4. However, since their impedance are frequency dependent, the theoretical 100% energy transmission is true only on one frequency point.

For SAW/BAW resonators, away from the resonance and anti-resonance frequencies, the resonator works as a capacitor. Thus, by replacing the capacitors in Figure 2.4 with SAW/BAW resonators, the L-matching network will still be lossless in a certain frequency range. However, near the resonance and anti-resonance frequency, Z_p is far away from the lossless transmission condition. The impedance mismatch of the network will be serious and it leads to deep notches on the transmission performance.

Further, to create more notches, the inductor in Figure 2.4 could also be replaced by the combination of SAW/BAW resonator and inductor. Figure 2.5 shows four possible structures of impedance converters, which are also used in the ladder topology band reject filters [2.2][2.3]:

(a) the serial arm is a serial connection of inductor and SAW/BAW resonator for the left port input impedance is smaller than right side one;

(b) the parallel arm is a parallel connection of inductor and SAW/BAW resonator for the left port input impedance is larger than right side one;

(c) the serial arm is a parallel connection of inductor and SAW/BAW resonator for the left port input impedance is smaller than right side one;

(d) the parallel arm is a serial connection of inductor and SAW/BAW resonator for the left port input impedance is larger than right side one.

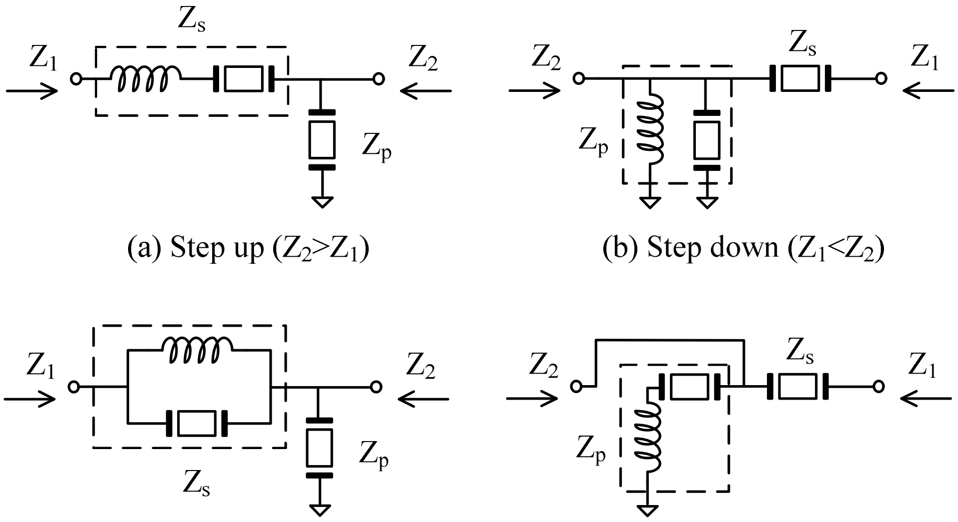

(c) Step up (Z_2>Z_1)   (d) Step down (Z_1<Z_2)

Figure 2.5 Basic L-matching network including SAW/BAW resonators

It seems these four structures should have similar performance as bandstop filters. However, for the inductors in practical use are usually not accurate enough, the sensitive transition band should not be influenced by the inductor value. In structure (a), the impedance of the serial resonator will be very large in stopband, so the contribution of the serial inductor could be neglect. In structure (b), the impedance of the parallel resonator will be very small in stopband, so the contribution of the parallel inductor could also be neglect. However, in structure (c), if anti-resonant on the serial arm is needed, which is the condition of stopband, the anti-resonance frequency will depend on the value of the inductor. For the same reason, the resonance frequency of the parallel arm in structure (d) will depend on the inductor value again. Although the inaccuracy of inductor value will also influence the passband performance of structure (a) and (b), the L-matching network passband position is much more insensitive, and the designed passband specification is usually not so strict. Thus, in this thesis, structure (a) and (b) are selected as the basic cell for the notch filter.

Assume the characteristic impedance of two ports are pure real. The transmission coefficient S_{21} of the network is given by

$$S_{21} = \frac{2\sqrt{R_1 R_2^{-1}}}{(R_1 + Z_S)(R_2^{-1} + Z_p^{-1}) + 1} \tag{2-1}$$

where R_1=Re[Z_1], R_2=Re[Z_2]. As discussed above, notch appears and S_{21} approaches zero when Z_s is extremely large on its anti-resonance frequency or Z_p is close to zero on its resonance frequency.

2.3.2 Passband characteristics

When the impedance of parallel arm and serial arm are well designed, the two ports are both matched, then the transmission could be lossless and the following conditions are satisfied:

$$Z_s = \pm jR_2\sqrt{r(1-r)} \tag{2-2}$$

$$Z_p^{-1} = \pm jR_2^{-1}\sqrt{r^{-1}-1} \tag{2-3}$$

where the double signs are in same order, r is the impedance ratio of two ports (R_1/R_2) and r should be smaller than unity because the left sides of equation are pure imaginary. Then (2-1) reduces to

$$|S_{21}|_{\max} \approx \frac{1}{1 + \frac{R_1^{-1}}{2}R_s + \frac{R_2}{2}G_p} \tag{2-4}$$

where R_s=Re[Z_s] and G_p=Re[Z_p^{-1}]. Since dielectric and ohmic losses are not significant in present SAW/BAW resonators, R_s and G_p will be mainly determined by the finite quality factor of inductors Q_L. To study the performance of the filter in passband, SAW/BAW resonators in series and parallel arms are replaced with capacitors, C_{0s} and C_{0p}, respectively, because the SAW/BAW resonators act as capacitors far away from its resonance and anti-resonance frequencies. Figure 2.6 shows the corresponding circuit for passband, where R_s and G_p are two kinds of equivalent resistance of the inductor, while $R_s = j\omega L_I / Q_L$ and $G_p = 1 / j\omega L_I Q_L$.

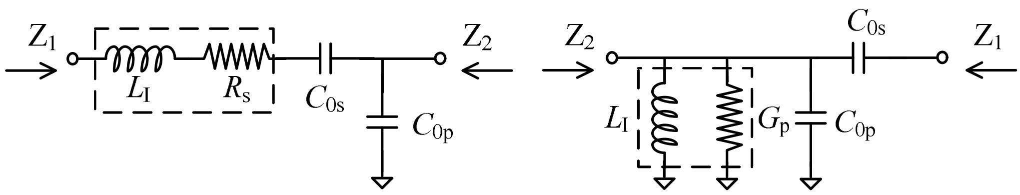

(a) Step up (Z2>Z1)   (b) Step down (Z1<Z2)

Figure 2.6 L-matching network with lumped elements

First, the influence of the inductor quality factor is discussed. Figure 2.7 shows the $|S_{21}|$ of structure in Figure 2.6(a) with the inductor quality factor Q_L increasing from 25 to 100. The horizontal axis is the frequency deviation from the matching frequency f_c, which satisfies the conditions given by (2-2) and (2-3). The result indicates that the insertion loss of passband decreases rapidly with the increase of Q_L, and the decreasing speed significantly drops (less than 0.1 dB) when Q_L is larger than 50. It indicates that to keep the passband insertion loss small, general commercial lumped inductors are enough to fulfill the requirement.

Next, it seems there are 6 variates in Figure 2.6 to design. However, their values are related with each other when the matching condition in (2-2) and (2-3) are fulfilled.

Following research fixed R_1 to 50 Ω, Q_L to 50 and center frequency to 750 MHz. Then there are two choices, fix the combined capacitor (C_{0s} in Figure 2.6(a) and C_{0p} in Figure 2.6(b)) or fix the individual capacitor (C_{0p} in Figure 2.6(a) and C_{0s} in Figure 2.6(b)). The first choice will cause C_{0s}/C_{0p} depending on r while the second choice requires r be a constant.

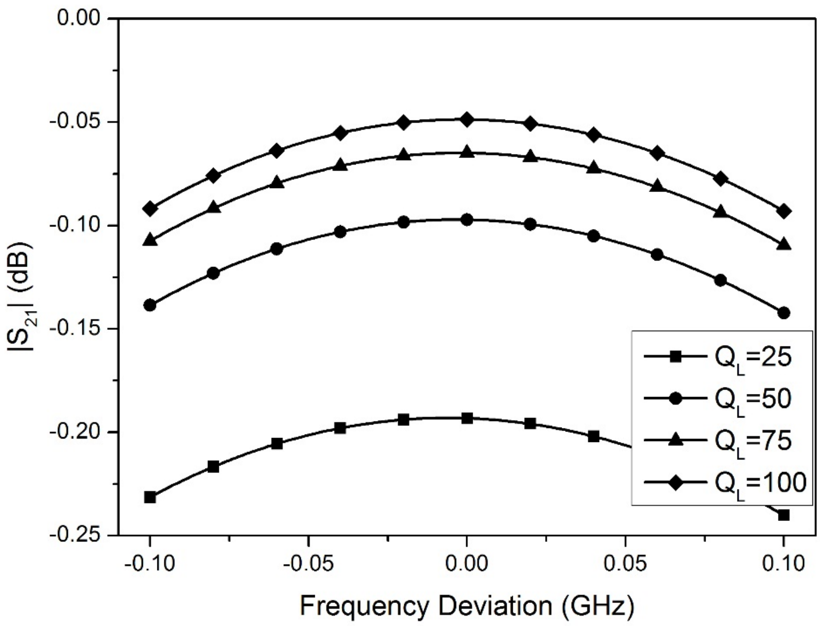

Figure 2.7 Performance of L-network with various inductor quality factor

Figure 2.8 shows the $|S_{21}|$ variating with r when the combined capacitor is fixed. As shown in the figure, the insertion loss grows and the passband flatness becomes worse with the decreasing of r. This is because when r is smaller, the impedance difference between two ports is lager. Then the impedance matching is possible only for a narrower frequency range. At the same time, the inductor value will become larger, with the same Q_L, the real part of the inductor also increased, which leads the insertion loss grows.

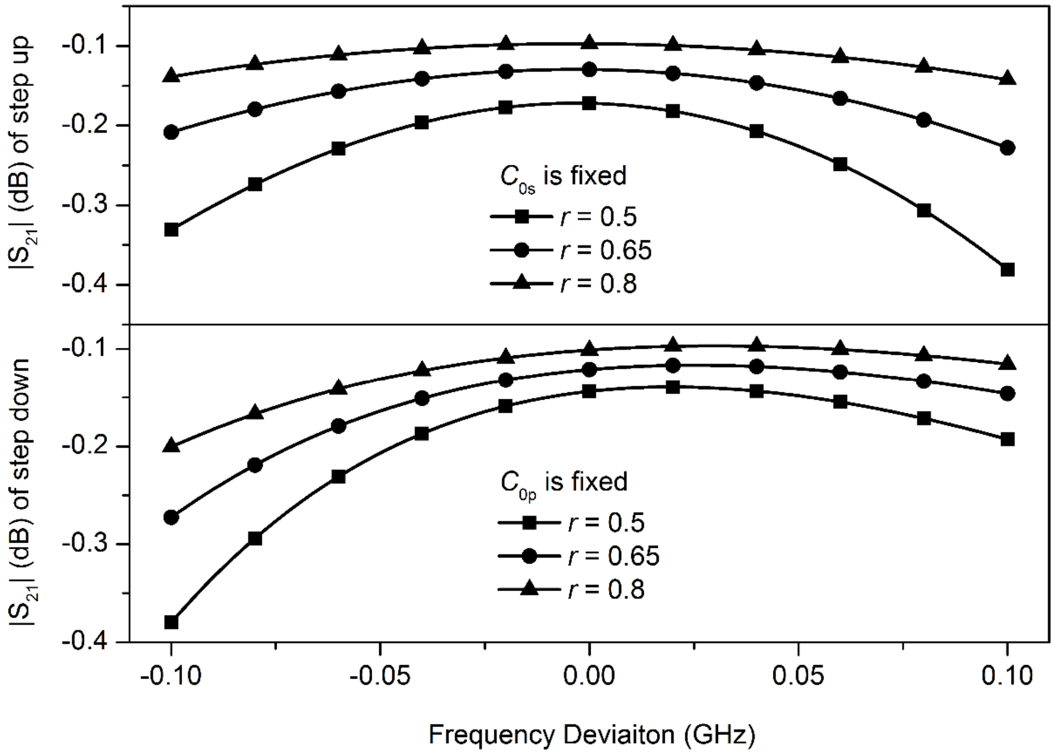

Figure 2.8 Pass band characteristic of L-matching network

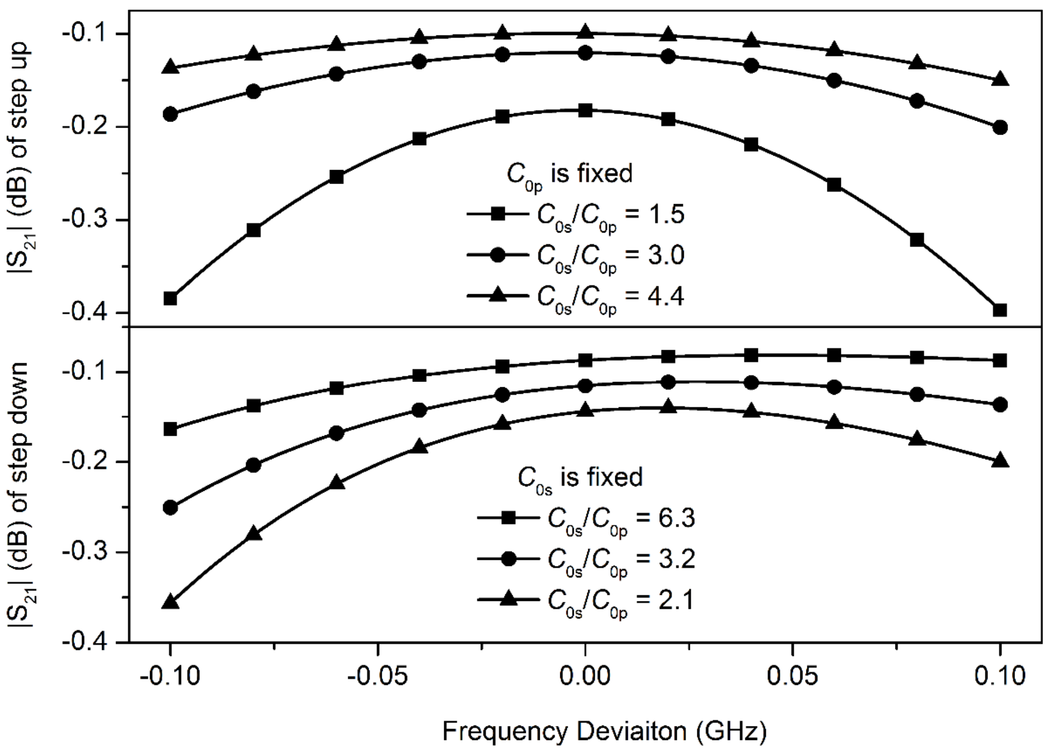

Figure 2.9 Pass band characteristic of L-matching network

Figure 2.9 shows the $|S_{21}|$ variating with C_{0s}/C_{0p} when the individual capacitor is fixed. As shown in the figure, the insertion loss grows and the passband flatness becomes worse with the decreasing of C_{0s}/C_{0p}. The mechanism of insertion loss growing is the same with Figure 2.8, the value of inductor grows with the decreasing of C_{0s}/C_{0p}. On the other side, both in configuration (a) and (b), the influence of the combined capacitor to the circuit will decrease when C_{0s}/C_{0p} decreased. Because the impedance of the combined arm is composed by the inductor and the combined capacitor, and the influence of capacitor is always negative to the circuit impedance. Thus, smaller influence of combined capacitor corresponds to lower insertion loss.

2.3.3 Stopband considerations

Next, rejection characteristics near the resonance frequencies are discussed. For the purpose, each resonator in Figure 2.5 (a) and (b) is modeled by the simple LCR model in Figure 2.10,

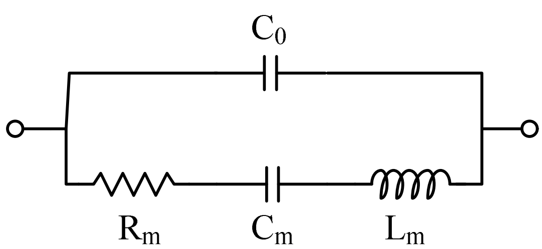

Figure 2.10 LCR model of SAW/BAW resonator

where L_m, C_m and R_m are the motional inductance, capacitance, and resistance, respectively, and C_0 is the clamped capacitance. The resonance frequency f_r is given by $1/2\pi(L_mC_m)^{0.5}$, while the anti-resonance frequency f_a is given by $f_r(1+\gamma^{-1})^{0.5}$, where γ

(= C_0/C_m) is the capacitance ratio. The resonance and anti-resonance quality factors, Q_r and Q_a, respectively, are given by $2\pi f_r L_m/R_m$ and $2\pi f_a L_m/R_m$ for this case.

Two dips occur near the resonance f_{rp} of the parallel resonator and the anti-resonance f_{as} of the series resonator. When f_{rp} and f_{as} are not close to each other, the term $Z_s Y_p$ in (2-1) is negligible. $|S_{21}|$ at these frequencies and -3 dB rejection bandwidths contributed by each resonator are approximately given by

$$\left|S_{21}\right| \ (\text{at} f = f_{\text{as}}) \approx \frac{4\pi f_{\text{as}} C_{0\text{s}} R_{\text{i}} \gamma}{Q_{\text{a}}}, \tag{2-5}$$

$$\left|S_{21}\right| \ (\text{at} f = f_{\text{rp}}) \approx \frac{\gamma}{\pi f_{\text{rp}} C_{0\text{p}} R_{\text{o}} Q_{\text{r}}}, \tag{2-6}$$

$$\text{BW}_{\text{s}} \approx \frac{1}{4\pi C_{0\text{s}} R_{\text{i}} \gamma}, \tag{2-7}$$

$$\text{BW}_{\text{p}} \approx \frac{\pi f_{\text{rp}}^2 C_{0\text{p}} R_{\text{o}}}{\gamma}, \tag{2-8}$$

where C_{0p} and C_{0s} are C_0 of the parallel and series resonators, respectively. BW_s and BW_p are the bandwidth contributed by the serial and parallel resonators, respectively. This analysis shows rough characteristics of a single resonator which will be used for further design. When these two nulls are placed in proximity, the transition bands of the two resonators will overlap, and a bump occurs. Provided that the resonator Q is somewhat large, the attenuation level A_e is determined by this bump height, which becomes large with an increase in the frequency separation d between the two nulls. On the other hand, the total transition bandwidth BW_e is also determined by d. Figure 2.11

shows a designed example with the structure in Figure 2.5 (b), where r=0.69, γ=15, and Q_r=Q_a=500 while d is swept from 5 MHz to 20 MHz. It is seen that smaller d makes the dip levels deeper and the bandwidth smaller. Anyway, A_e and BW_e are in tradeoff.

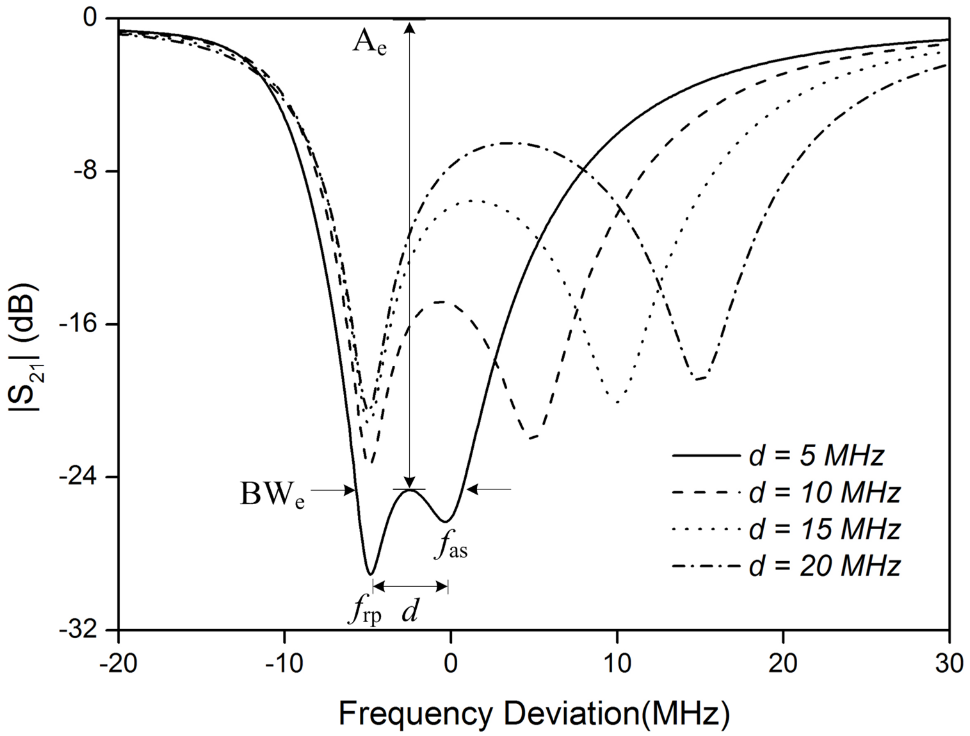

Figure 2.11 Bandwidth and attenuation of reject band variation with d

Figure 2.12 compares the result shown in Figure 2.11 when d is 10 MHz with results when one of the resonators is replaced with a simple capacitor. The topologies (a.1) to (a.3) are equivalent with the legends in the figure. So is (b.1) to (b.3). These results reveal that the following two synergy effects appear when two nulls are placed in proximity.

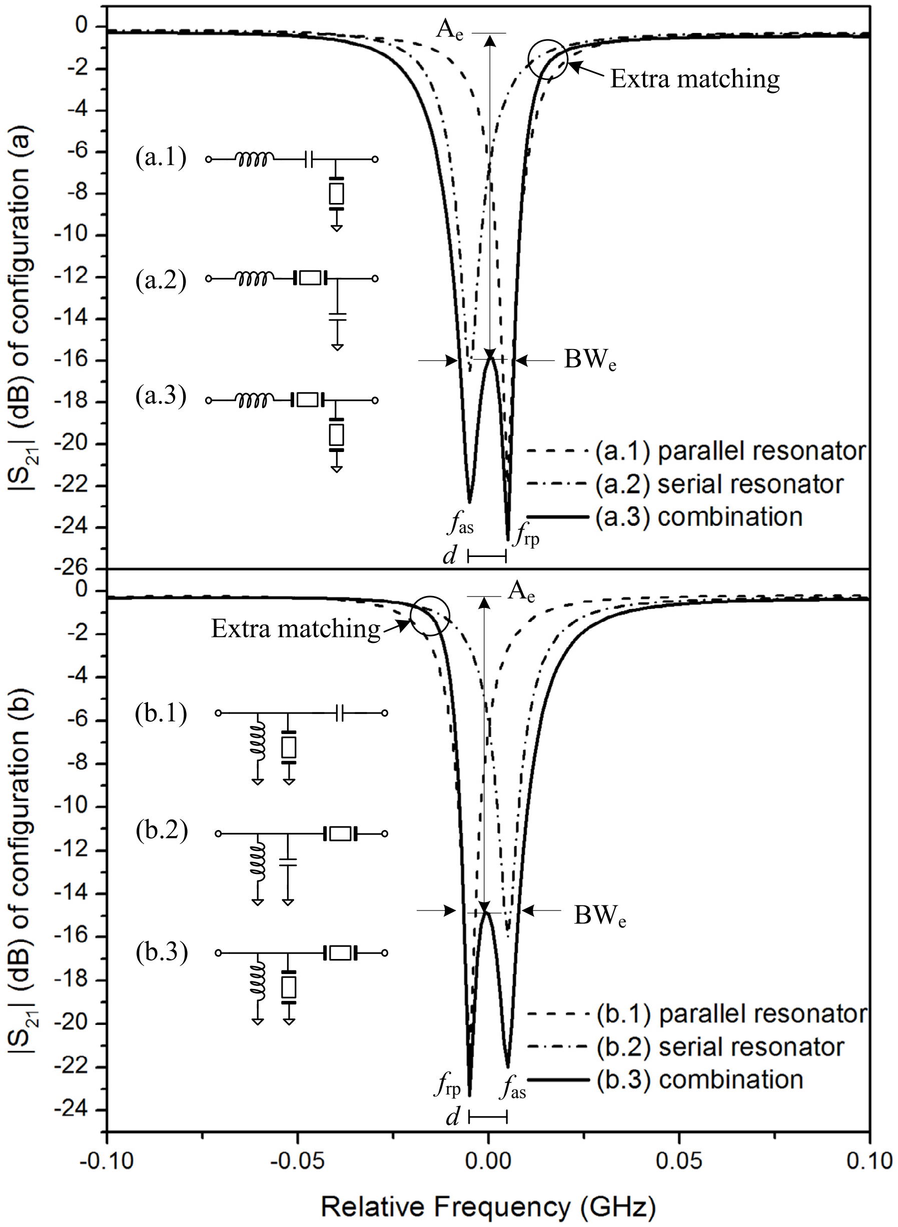

Figure 2.12 Rejection band characteristics of L-networks when two resonators are combined

(i) The upper edge of the rejection band becomes steep for the configuration (a). This is caused by fulfillment of (2-2) and (2-3) at a frequency just above the upper edge where the series resonator is capacitive and the parallel one is inductive. As a tradeoff, the lower edge becomes gradual. This effect also occurs to the configuration (b). In this case, the lower edge becomes steep while the upper edge becomes gradual.

(ii) For the configuration (a), the dip at f_{as} is much deeper than the value given by (2-5) while that at f_{rp} is mostly equal to that given by (2-6). Furthermore, the bump height in the rejection band is lower than the value given by a product of values given by (2-5) and (2-6). This is due to the term Z_sY_p in (2-3) is not negligible when the distance between the two nulls is small. These effects also occur to the configuration (b).

It should be noted that setting f_{rp}>f_{as} for the case (a) and setting f_{as}>f_{rp} for the case (b) offer negative effects: the bump become higher, and the two edges become unbalanced.

Figure 2.13 shows variation of $|S_{21}|$ of structure in Figure 2.5 (a) with the resonator quality factor Q from 1000 to 250. With the Q decrease, the passband band edges become round and two notches do shallow. However, A_e and BW_e do not change too much as expected, because d remains the same. Sharpness of the upper edge is mainly governed by the maximum value of Bode Q [2.4].

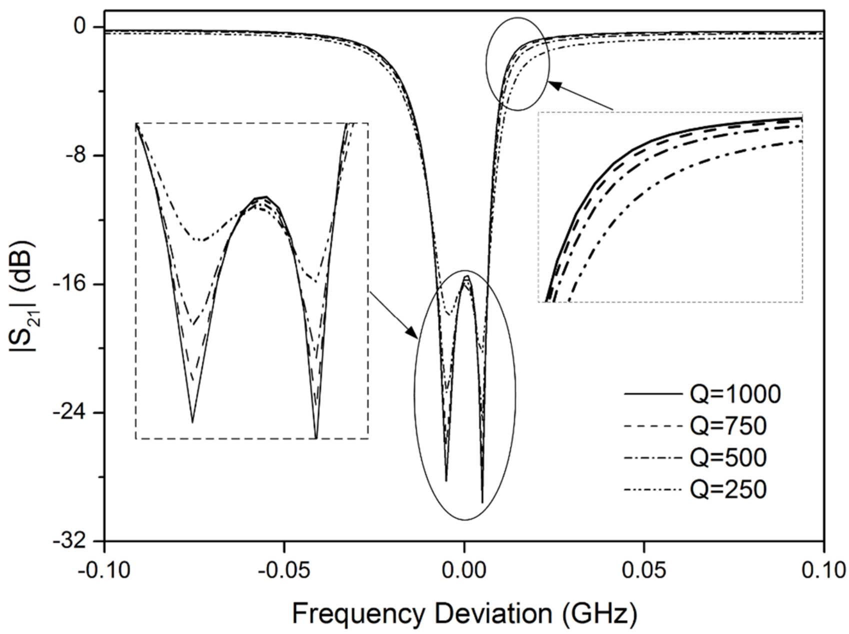

Figure 2.13 Performance of L-network with various resonator quality factor

2.4 Experimental Verification

To demonstrate the basic cell design, two one-port SAW resonators were fabricated, and band reject filters shown in Figure 2.12 were composed in a free circuit simulation tool called Qucs (Quite Universal Circuit Simulator) [2.5] using their measured admittance resonance characteristics.

Two resonators A and B were fabricated on 42°YX-$LiTaO_3$ (42-LT) substrate [2.6]. Copper was chosen as the electrode material, and the thickness was set at 300 nm. The SAW resonators employ the standard short-circuited (SC) reflector – interdigital transducer (IDT) – SC reflector structure shown in an inset of Figure 2.14. The IDT has 65 finger pairs while the number of electrodes is 30 for each reflector, The IDT periodicity for the resonator 1 and 2 are 5.854 μm and 5.697 μm, respectively.

Figure 2.14 depicts the measured admittance of the two resonators. The solid and dashed curves represent that of the resonator 1 and 2, respectively. Strong resonance can be seen at 638 MHz (1) and 654 MHz (2), which are caused by the main SAW mode. Resonance Q of these resonators was estimated as circa 450 from the fitting of these responses to the modified BVD (mBVD) model [2.7]. Spurious resonances can be seen at 881 MHz (1) and 912 MHz (2), which are caused by the bulk wave radiation intrinsic in 42-LT [2.8].

Then the measured S parameter files were loaded as a "black box" in Qucs, and the basic cell circuit was composed in combination with two built-in inductors. Their inductance was set at 137 nH from (2-2) and (2-3), and their Q factor was set at 50 on 600 MHz. In the design, r=0.69.

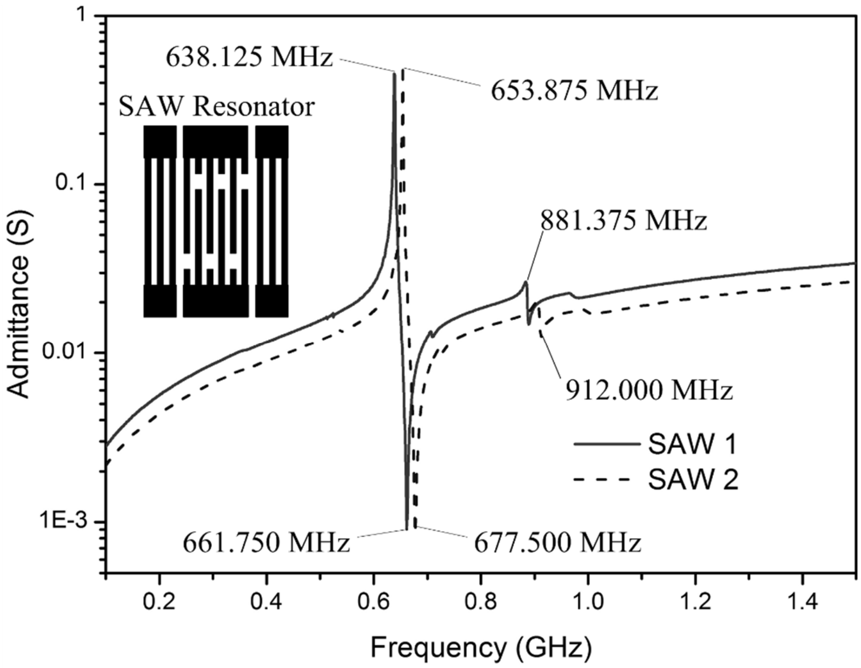

Figure 2.14 Measured admittance of the serial and parallel SAW resonators

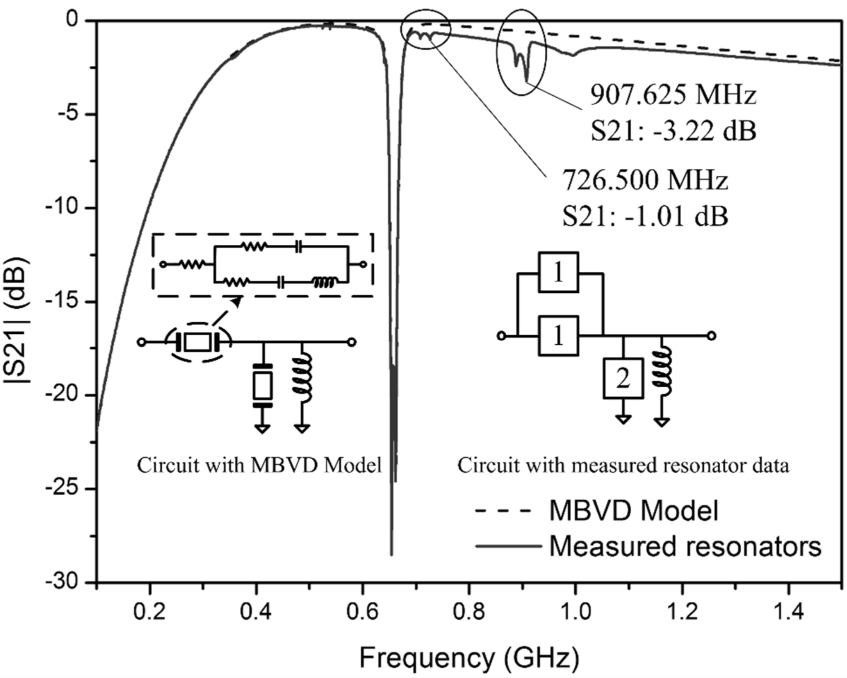

Figure 2.15 $|S_{21}|$ of the basic cell circuit (b) based on the MBVD model vs. the measured resonators

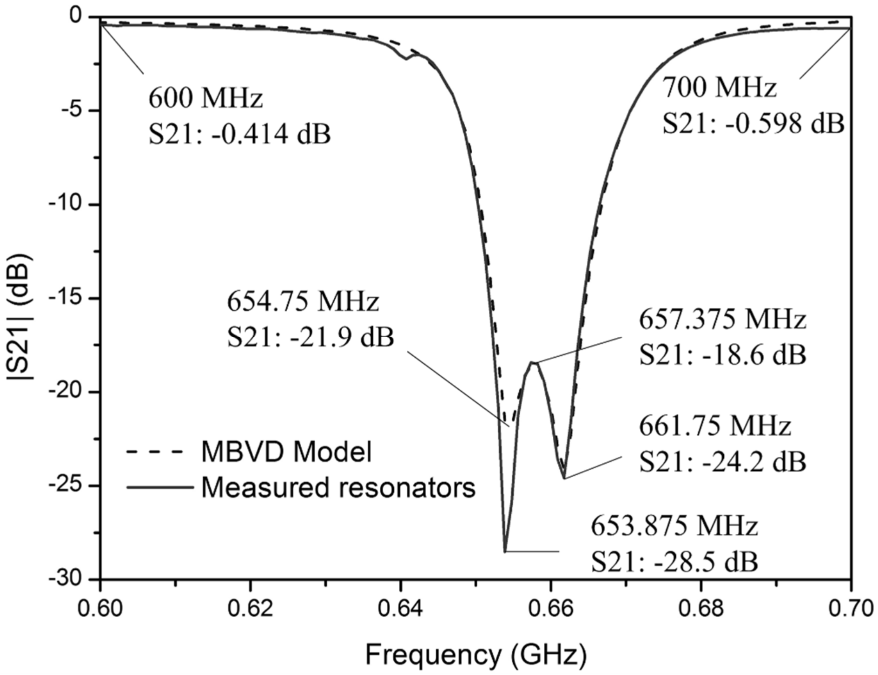

Figure 2.16 Zoom in of Figure 2.15 with a frequency range from 600 MHz to 700 MHz

Figure 2.15 and Figure 2.16 show calculated transmission response $|S_{21}|$ when the circuit shown in Figure 2.12 (b.3) was chosen. Here, a pair of resonator 1 are parallel connected to achieve double capacitance. This method is used to reduce the lithography area for each resonator. The rejection band with two dips can be seen at ~654 MHz and ~662 MHz, which correspond to the resonance frequency of the resonator 2 and the anti-resonance frequency of the resonator 1, respectively. For comparison, $|S_{21}|$ calculated by using the mBVD model is also shown. In this calculation, the resonance Q was limited to 250 intentionally. Nevertheless, this calculation agrees quite well with the original simulation except the dip depth at ~653 MHz, which is mainly determined by the anti-resonance Q of the series resonator. Although the resonator Q and assumed inductance Q was low (450 and 50, respectively), achieved insertion loss is relatively small.

Another notch is seen at ~907 MHz, which is caused by the bulk wave radiation. Use of other SAW substrates such as 128°YX-$LiNbO_3$ [2.9] may relax this problem.

Figure 2.17 and Figure 2.18 show calculated transmission response $|S_{21}|$ when the circuit shown in Figure 2.12 (a.3) was chosen. Here, a pair of resonator 2 are serial connected to reduce capacitance. The rejection band with two dips can be seen at ~654 MHz and ~662 MHz, which correspond to the resonance frequency of the resonator 2 and the anti-resonance frequency of the resonator 1, respectively. The simulated result using the measured admittance agrees well with the one obtained by using the mBVD model.

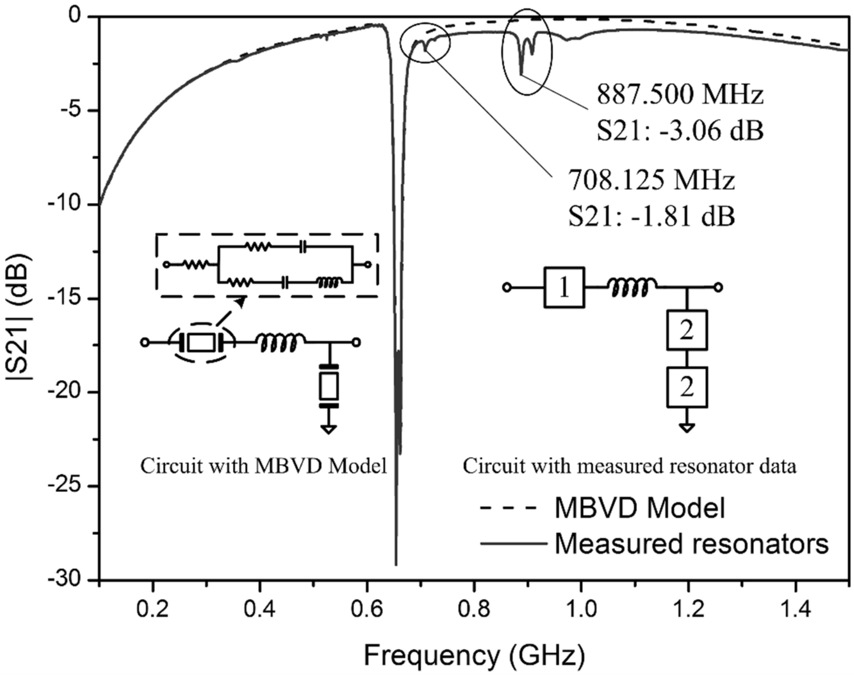

Figure 2.17 $|S_{21}|$ of the basic cell circuit (a) based on the MBVD model vs. the measured resonators

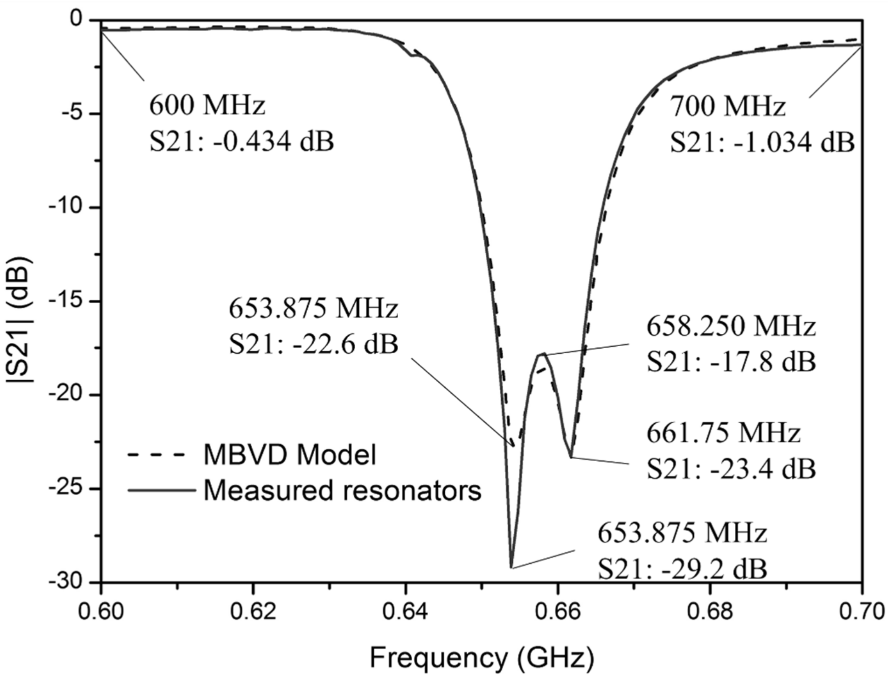

Figure 2.18 Zoom in of Figure 2.17 with a frequency range from 600 MHz to 700 MHz

2.5 Design of Multi-stage band reject filters

Since cascade connection of N-stages generates $2N$ nulls, their proper allocation enables the rejection band to be wider, deeper, etc. Cascading with mirror inversion makes the input and output impedance identical, and the circuit can be used as an isolated band reject filter. (2-7) and (2-8) indicate that the fractional bandwidth of SAW/BAW resonator is very narrow and is limited by γ or the electromechanical coupling coefficient K_e^2.

The bandwidth can be increased by cascading multiple stages and setting resonance frequencies appropriately. As an example, here a notch filter for a specification given in Table 2.1 is designed.

Table. 2.1 Design specification of the band reject filter

Freq.	Min	Typ	Max
470…603 MHz	-	-	2 dB
603…653 MHz	-	-	5 dB
703…748 MHz	10 dB	27 dB	-

The structure in Figure 2.5 (b) is selected as the basic cell of the band reject filter. Use of SAW resonators on 42-LT are assumed and γ is set at 15.

The discussion in Section II indicated larger r results in better insertion loss. However, if r is too close to unity, the capacitance given by (2-2) and (2-3) will be extremely large and impractical. As a compromise, here r is set at 0.69 which corresponds to C_{0s} = 8.2 pF. Location of resonance frequencies are adjusted so that the bump level is -27 dB, while the number of stages are adjusted so that the required rejection bandwidth is obtained.

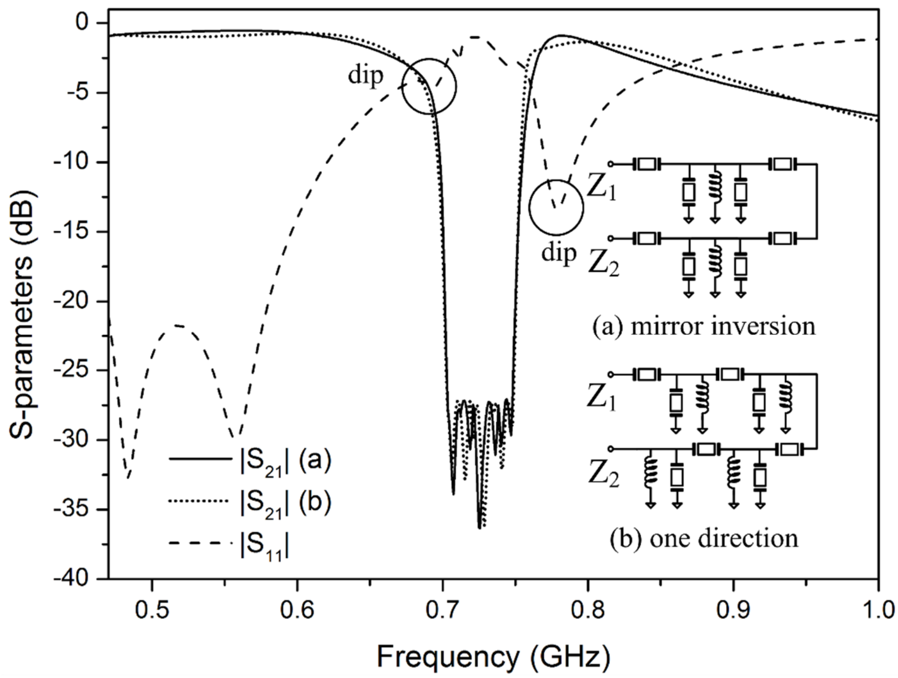

Figure 2.19 Performance of designed band reject filters

The designed result is shown in Figure 2.19. Two cascading methods are designed. For the design (a), the input and output impedance are both 50 Ω. The mirror inversion is applied, and the adjacent two inductors are combined to one. On the other hand, the input impedance is 50 Ω and the output impedance is 72.4 Ω for the design (b). For both cases, all the requirements given in Table are satisfied. The maximum insertion losses in 470-603 MHz and 603-653 MHz are 0.93 dB and 1.90 dB, respectively for the case (a), and are 0.82 dB and 1.54 dB, respectively for the case (b). Note that required Q factor of the resonators is 250 for this specification. The value is quite easy to realize.

As indicated in Figure 2.12, there are two dips in $|S_{11}|$ at frequencies close to the rejection band edges. They are the extra matching points mentioned in the last section. These points enhance the steepness of the transition band.

2.6 Conclusion

This chapter discussed design of a band reject filter composed of the impedance converters.

First, basic properties of the unit cell are studied. It was shown how the pass band insertion loss, rejection bandwidth and its attenuation level change with the design for a unit cell. It was found that when two notches are placed in proximity, two synergy effects occur: (i) an extra matching point appears on one side of the transition band. This make the insertion loss at the point smaller and the transition band steeper, and (ii) the dip level becomes deeper, and the total rejection level becomes better.

Then two SAW resonators were fabricated on 42-LT, and the filter operation was examined on the circuit simulator in combination with built-in inductors. The simulated result agrees well with the one based on mBVD model, and functionality of the basic cell design was demonstrated.

Finally, the wide rejection band filter was designed for the given specification. The rejection bandwidth was expanded by cascading multiple unit cells with different design. The designed performance revealed effectiveness of the design.

Reference

[2.1] X. Zhang, X. Ruan, H. Kim and C.K. Tse. "Adaptive active capacitor converter for improving stability of cascaded DC power supply system." *Power Electronics, IEEE Transactions on,* 28, 4 (2013) p. 1807

[2.2] S. Beaudin, C.Y. Jian, and D. Sychaleun. "A new SAW band reject filter and its applications in wireless systems." *Proc. IEEE Ultrason. Symp.* (2002) p. 147

[2.3] T. Bauer, M. Jungkunz and K. Wagner, "SAW Band Rejection Filters for Mobile Digital Television," *Proc. IEEE Ultrason. Symp.* (2008) p. 288

[2.4] D.A. Feld, R. Parker, R. Ruby, P. Bradley and S. Dong, "After 60 Years: A New Formula for Computing Quality Factor is Warranted," *Proc. IEEE Ultrason. Symp.* (2008) p. 431

[2.5] http://qucs.sourceforge.net/

[2.6] Kawachi, S. Mineyoshi, G. Endoh, M. Ueda, O. Ikata, K. Hashimoto and M.

Yamaguchi, "Optimal Cut for Leaky SAW on $LiTaO_3$ for High Performance Resonators and Filters," *IEEE Trans. Ultrason., Ferroelec. and Freq. Contr.,* 48, 5 (2001) p. 1442

[2.7] J. D. Larson, III, P.D. Bradley, S. Wartenberg, and R.C. Ruby, "Modified Butterworth-Van Dyke Circuit for FBAR Resonators and Automated Measurement System," *Proc. IEEE Ultrason. Symp.* (2000) p. 863

[2.8] Y. Satoh and O. Ikata, "Ladder-type SAW Filter and Its Application to High Power Devices," *Advances in Surface Acoustic Wave Technology, Systems and Applications,* 1, edited by C.C.W. Ruppel and T.A. Fjeldly (World Scientific, 2000) p. 273

[2.9] Y. Wang, M. Solal, T. Kook, J. Briot, B. Abbott, A. Chen, T. Daniel, S. Malocha, K. Qin, and K. Steiner, "A Zero TCF Band 13 SAW Duplexer," *Proc. IEEE Ultrason. Symp.* (2015) DOI: 10.1109/ULTSYM.2015.0092

3 Multimode filters using one-port SAW/BAW resonators

3.1 Introduction

This chapter discusses the possibility of realizing multimode filters composed of multiple single-mode resonators.

After a brief introduction of DMS filter design, the multimode filter operation and design principle are given. It is shown that excellent filter characteristics are achievable by combining multiple single-mode resonators with identical capacitance ratios provided that their resonance frequencies and clamped capacitances are set properly.

Next, the influence of the balun performance is investigated. It is shown that the total filter performance is significantly degraded by balun imperfections such as the common-mode rejection. Then, two circuits are proposed to improve the common-mode rejection, and their effectiveness is demonstrated.

3.2 Design principle of traditional DMS filters

Designing of the traditional DMS filter is based on the acoustic coupling between its symmetric and anti-symmetric modes. Figure 3.4 shows the typical structure of a DMS filter, which contains two IDT and two reflectors. In the figure, L_I and L_r represent the length of IDT region and reflector region, L_T and L_g represent the gap length between two IDT and IDT with reflector, respectively. This structure could excite two modes simultaneously, the symmetric mode is shown in dashed line and the anti-symmetric mode is shown in dot line.

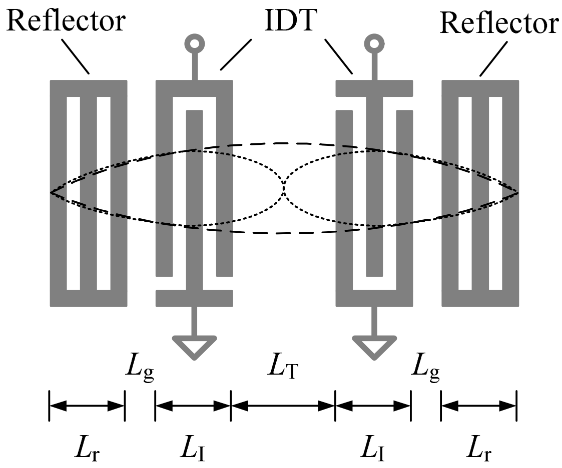

Figure 3.1 Typical DMS filter structure with two possible excited modes

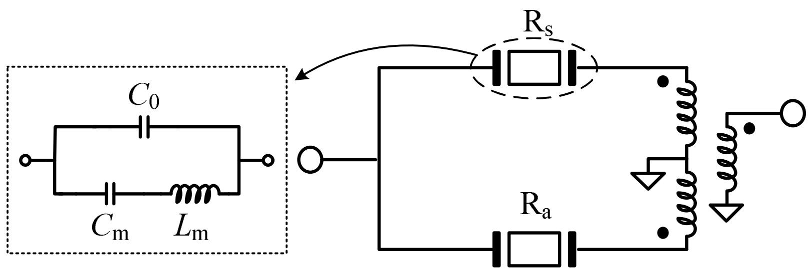

Figure 3.2 DMS filter equivalent circuit

Figure 3.2 shows the equivalent circuit of the DMS filter, where R_s and R_a represent the equivalent model of the symmetric and anti-symmetric modes, respectively. Each model could be further expressed by the circuit in the inset, which is similar to a single resonator. The location and separation of the resonance and anti-resonance frequencies of R_s and R_a are mainly determined by L_I and L_T.

Figure 3.3 shows the DMS filter characteristics variating with the admittance of R_s and R_a, where f_{sr} and f_{sa} represent the resonance and anti-resonance frequency of R_s, f_{ar} and f_{aa} represent the ones of R_a. In the passband, R_s should work near f_{sr} to obtain impedance close to zero, which R_a should work near f_{aa} for very high impedance. So that most of the energy flows through R_s, and low loss transmission is achieved. Out of passband, the two resonators act as capacitors and are coupled with 180° phase shift in circuit. Since the static capacitance of R_s and R_a are designed equal, the signal from two paths are cancelled and the filter output will be very small.

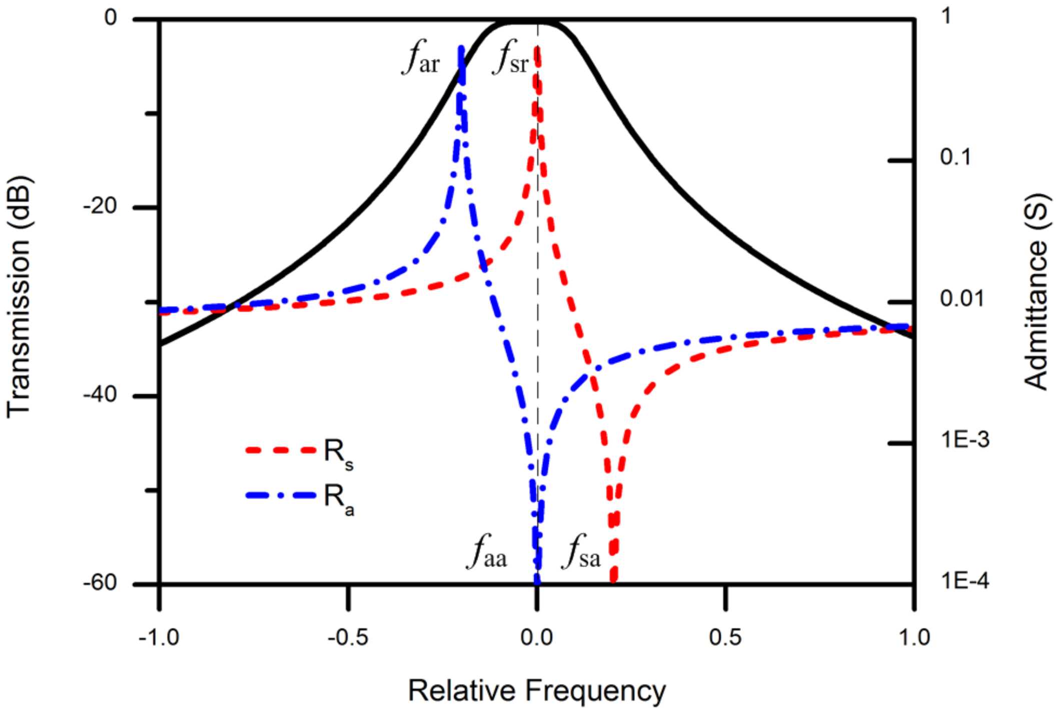

Figure 3.3 DMS filter characteristics variating with the symmetric and anti-symmetric resonator admittance

3.3 Electrically coupled multimode filter

Different from the DMS filter, this multimode filter applies electrical coupling. Figure 3.4 (a) shows the equivalent circuit of a multimode filter, where R_1 and R_2

represent the resonators supporting multiple resonances. Attempt has been made to compose this circuit using multiple single-mode resonators, which are realizable using RF SAW/BAW technologies in Figure 3.4 (b).

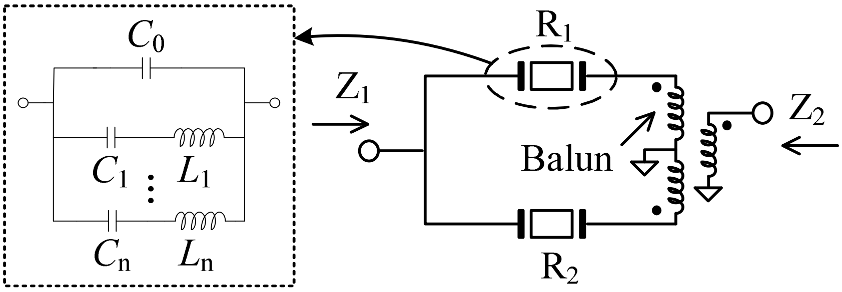

(a)

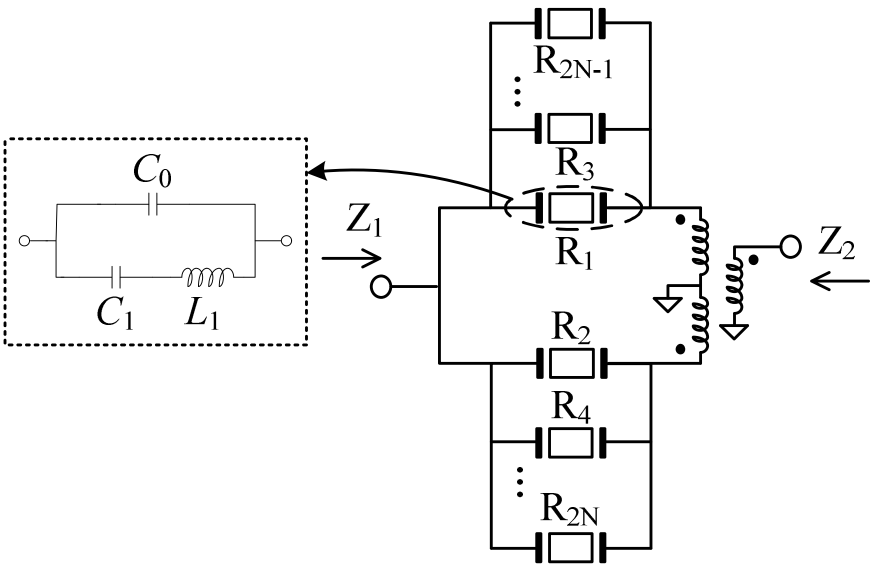

(b)

Figure 3.4 Equivalent circuit of multimode filter: using (a) multimode resonators and (b) multiple single-mode resonators

First, the design of the filter structure shown in Figure 3.4 (a) is discussed. The LCR model shown in the inset is used as a model of multimode resonators [3.1]. In the following numerical calculations, the quality factor Q and the ratio of capacitance γ of resonator elements are set at 2,000 and 15, respectively.

The basic design rule of this filter is similar to that of the lattice filter [3.2]: (i) the clamped capacitance C_0 of these resonators is $1/4\pi f_c R_0$, where R_0 is the peripheral circuit impedance and (ii) the resonance frequency of resonator 1 (R_1) coincides with the anti-resonance frequency of resonator 2 (R_2) and/or vice versa.

Figure 3.5 shows a design example with two single-mode resonators. In the figure, the admittances of R_1 and R_2, which are Y_1 and Y_2, are also shown. Lossless transmission is possible at the frequency where condition (ii) is fulfilled. The passband width is given by the loaded Q of the circuit, which is basically determined by the γ of resonators. It is known that the passband width can be increased slightly by making these resonance frequencies slightly different [3.2].

The steepness of the filter cutoff is inherently limited by the number of frequencies satisfying condition (ii). There are three techniques to improve the steepness. The first is increasing the γ of the resonators, which will decrease the pass bandwidth at the same time. The second is cascading multiple filter sections. This is simple but requires multiple baluns. The third is using resonators that support multiple resonances to satisfy condition (ii) at multiple frequencies.

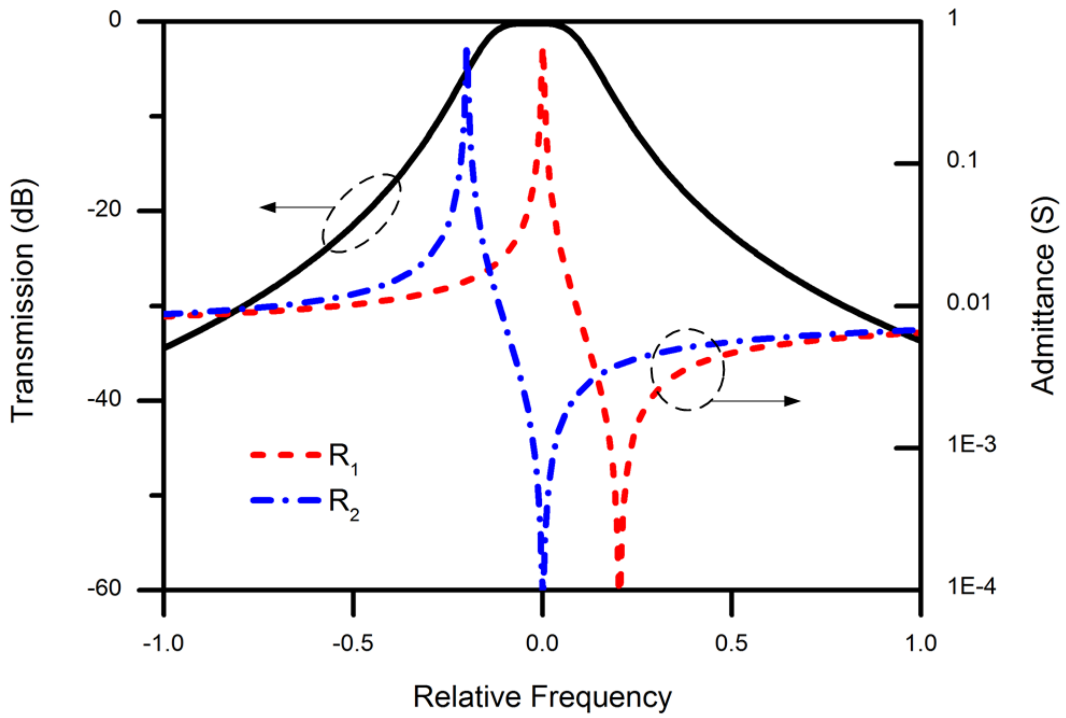

Figure 3.5 Performance of designed multimode resonators composed of two single-mode resonators

Next, the case is discussed where R_1 and R_2 support two resonances each. The resonance frequencies of resonator 1 are designated as f_1 and f_3 and those of resonator 2 as f_2 and f_4. Then, the design rules require that resonator 1 causes anti-resonances at f_2 and f_4, and resonator 2 causes anti-resonances at f_3 and f_5. Thus, under the design rules, Y_1 and Y_2 can be expressed as

$$Y_1 = j\omega C_0(1+\gamma^{-1})\frac{\left[1-\left(f/f_2\right)^2\right]\left[1-\left(f/f_4\right)^2\right]}{\left[1-\left(f/f_1\right)^2\right]\left[1-\left(f/f_3\right)^2\right]}, \tag{3-1}$$

$$Y_2 = j\omega C_0(1+\gamma^{-1})\frac{\left[1-\left(f/f_3\right)^2\right]\left[1-\left(f/f_5\right)^2\right]}{\left[1-\left(f/f_2\right)^2\right]\left[1-\left(f/f_4\right)^2\right]}, \tag{3-2}$$

where $\omega = 2\pi f$. The following condition is introduced so that Y_1 and Y_2 are almost equal at frequencies much higher than the passband:

$$\frac{f_1^2 f_3^2}{f_2^2 f_4^2} = \frac{f_2^2 f_4^2}{f_3^2 f_5^2}. \tag{3-3}$$

When this condition is not applied, two zeros appear in the transmission response at frequencies satisfying Y_1=Y_2. They can be used to enhance the sharpness of the passband edges as a tradeoff of the deteriorated out-of-band rejection far from the passband [3.3].

Here, f_i are set as $f_n = \sqrt{c} f_{n-1}$ to satisfy (3-3). Then, (3-1) and (3-2) can be respectively rewritten as

$$Y_1 = j\omega C_1 \left[1 + \frac{\gamma^{-1}}{1-\left(f/f_1\right)^2} \right] + j\omega C_3 \left[1 + \frac{\gamma^{-1}}{1-\left(f/f_3\right)^2} \right], \tag{3-4}$$

$$Y_2 = j\omega C_2 \left[1 + \frac{\gamma^{-1}}{1-\left(f/f_2\right)^2} \right] + j\omega C_4 \left[1 + \frac{\gamma^{-1}}{1-\left(f/f_4\right)^2} \right], \tag{3-5}$$

when

$$f_n = \left(\gamma^{-1}+1\right)^{(n-1)/4} f_1 \quad \left[c = \left(\gamma^{-1}+1\right)^{1/2} \right], \tag{3-6}$$

$$C_1 = C_2 = C_0(1+\gamma^{-1}) \frac{c^2+c+1}{(c+1)^2}, \tag{3-7}$$

$$C_3 = C_4 = C_0(1+\gamma^{-1}) \frac{c}{(c+1)^2}. \tag{3-8}$$

Namely, Y_1 and Y_2 can be realized by using the configuration shown in Figure 3.4 (b) which contains four single-mode resonators with identical γ values. The resonance frequency and clamped capacitance of the n-th resonator should be set as f_n and C_n, respectively, given by (3-6)~(3-8).

Figure 3.6 shows the transmission response of the filter composed of four single-mode resonators along with the synthesized Y_1 and Y_2. Comparison of this figure with Figure 3.5 indicates that the passband is flatter and wider and the cutoff is steeper owing to the triple-mode operation.

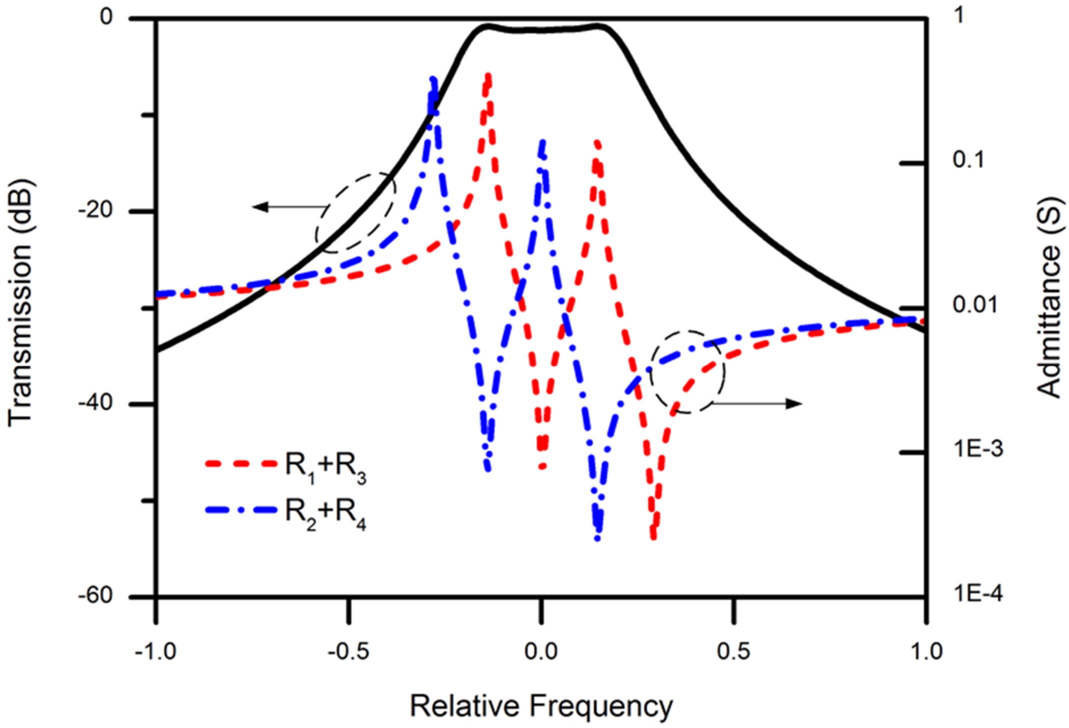

Figure 3.6 Performance of designed multimode resonators composed of four single-mode resonators

Note that the setting of $f_n = \sqrt{c} f_{n-1}$ is not mandatory. Even when f_n (n=1~5) are set differently, Y_1 and Y_2 can be realized by combining four single-mode resonators, although the γ values of the resonators will not be identical. The same design protocol can be applied to cases where R_1 and R_2 each support N resonances. Ideally, the filter response improves with increasing N. However, it also results in the increased insertion loss and dully passband edges owing to the finite resonator Q.

3.4 Impact of balun performance

Next, it is examined how balun performance influences filter performance. The commercial balun LDM0Q2G5010BE005 from MURATA was chosen for the analysis [3.4]. Its impedances are 50 and 100 Ω for the one unbalanced and two balanced ports, respectively. The typical passband and minimum insertion loss are 2500±200 MHz and 0.57 dB, respectively. Figure 3.7 shows the transmission characteristics, which were given in the touchstone format from MURATA. It is seen that the difference between S_{21} and S_{31}, giving the common-mode suppression, increases with the frequency separation from 2,500 MHz. This means that the device exhibits the balun function in a relatively narrow frequency range of approximately 2,500 MHz.

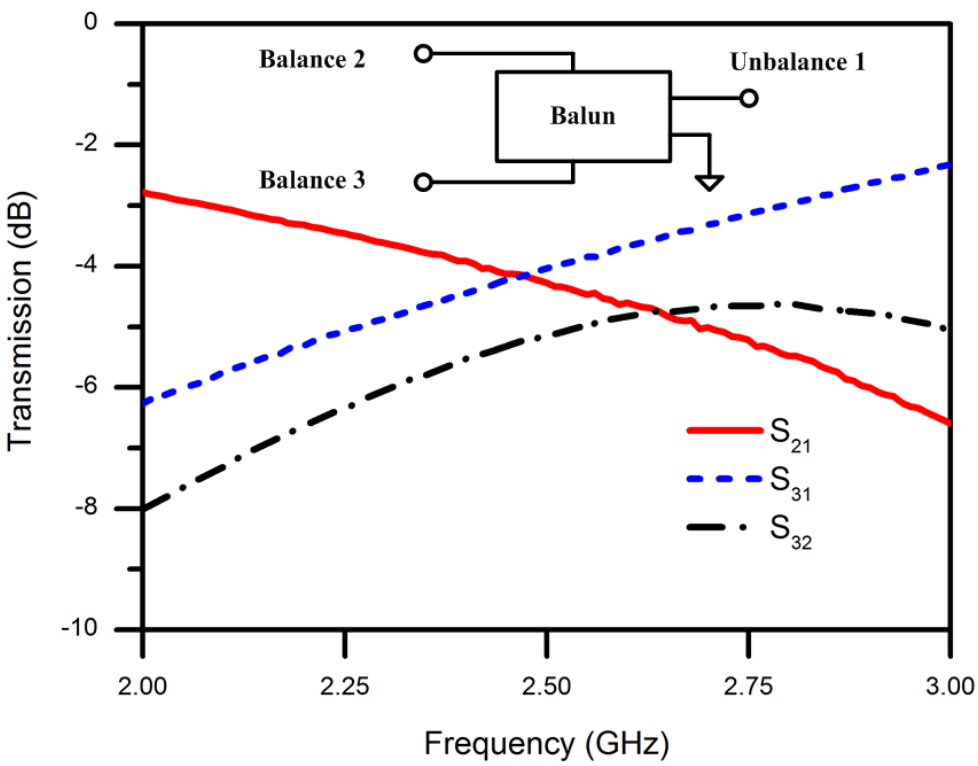

Figure 3.7 Transmission characteristics of the commercial balun from MURATA

Then, a filter with a center frequency of 2,500 MHz was designed following the rules described in Sect. 2, and its ideal balun was replaced with the touchstone format data of the balun on a free circuit simulator Qucs (Quite Universal Circuit Simulator) [3.5].

Figure 3.8 shows the filter characteristics. In the figure, the simulated result for the ideal balun is also shown. It is seen that the balun imperfection causes significant deterioration of the filter characteristic.

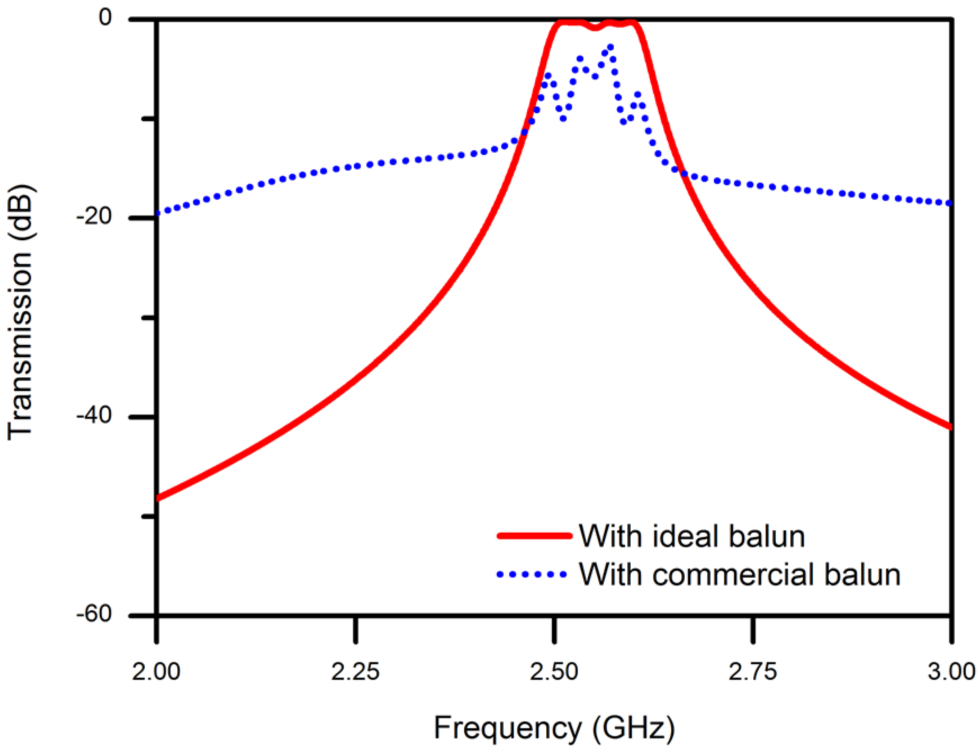

Figure 3.8 Performance of the designed multimode filter with the commercial balun

Here, the circuit (balance enhancer) shown in Figure 3.9 is introduced to improve the common-mode rejection. For the differential mode, the circuit corresponds to the π-type equivalent circuit of transmission lines, since no voltage drop occurs in L_p. Thus, 100% power transfer is possible between the input and output ports at a frequency under the proper settings of L_s and C_p. On the other hand, for the common mode, L_p causes a series resonance with C_p. This forms a notch at this resonance frequency only for the common-mode response. Different values can be set for the left L_p and right L_p to form two notches at different frequencies.

Figure 3.10 shows transmission characteristics of this circuit with a center frequency of 2.5 GHz in the differential and common modes. Here, the left L_p and right L_p are set to be equal, and L_p, C_p, and L_s were chosen to be 4.77 nH, 8.49 pF, 4.77 nH, respectively, and the Q factor of the inductors was set at 50 at 2.5 GHz.

It is seen that good common mode rejection is achievable while the differential mode is not influenced too much with small losses. Owing to the intrinsic low-pass nature of this circuit, the common-mode rejection becomes worse at low frequencies.

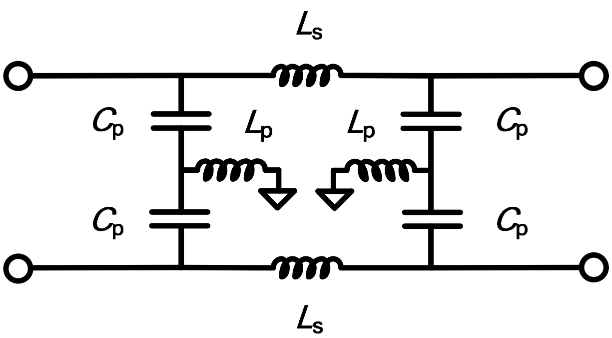

Figure 3.9 Low-pass-type balance enhancer

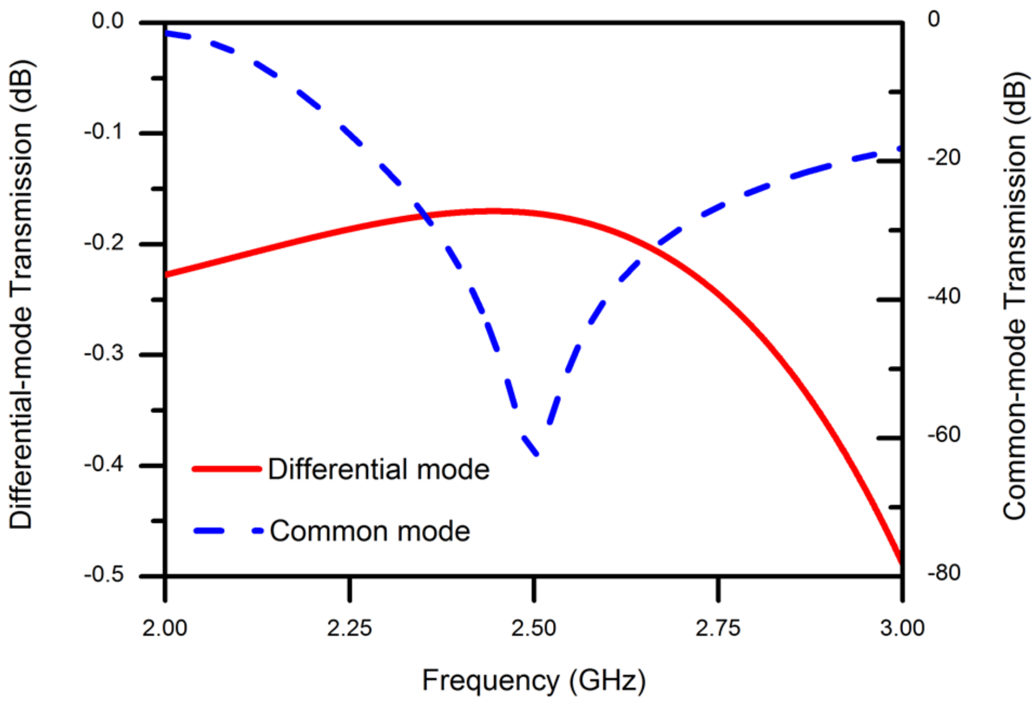

Figure 3.10 Transmission characteristics of low-pass balance enhancer in differential mode and common mode

Figure 3.11 shows the transmission characteristics when the circuit is inserted in the filter topology as shown in the inset. Owing to the improved common-mode rejection, the filter response close to the original design can be achieved. It is interesting to note that the intrinsic low-pass characteristic of the enhancer does not significantly affect the total performance, and good out-of-band rejection is achieved at frequencies lower than the passband. Two notches appear on the blue curve at 2.34 and 2.69 GHz. These notches enhance the sharpness of the transition bands but deteriorate the out-of-band rejection far from the passband. They are related to the imperfection of the balun used, which may be difficult to control.

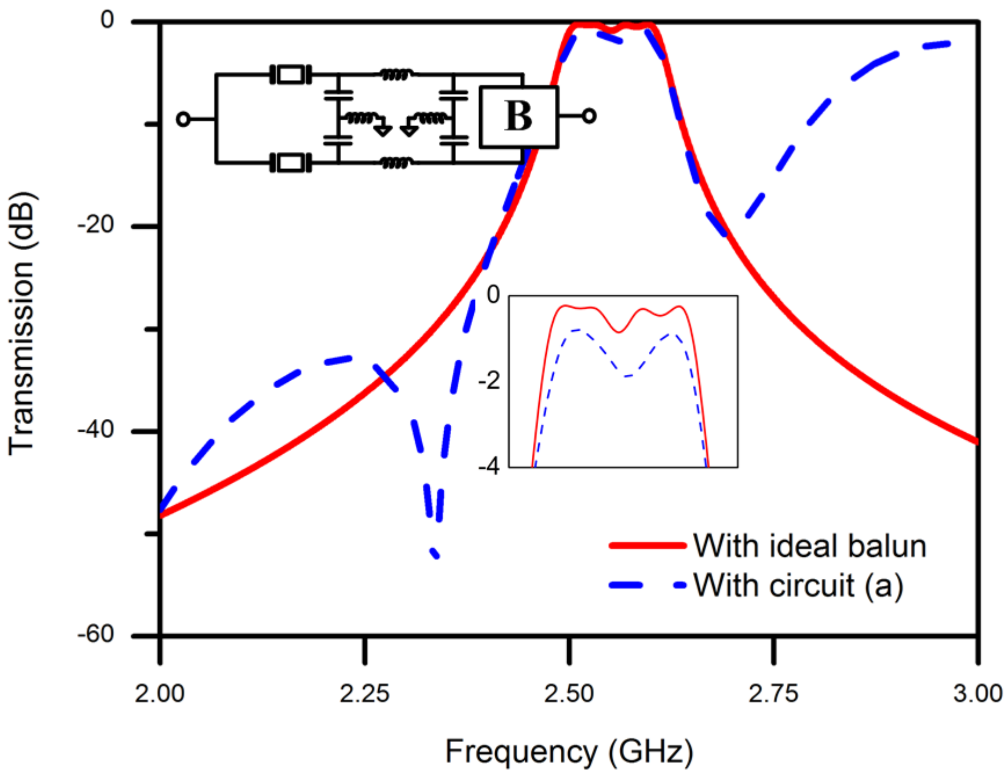

Figure 3.11 Performance of filter with low-pass balance enhancer and commercial balun from MURATA

On the other hand, the out-of-band rejection is not good at frequencies higher than the passband. Further investigation indicated that this degradation is due to that of the common-mode rejection caused by the interaction between the enhancer and the balun.

Figure 3.12 shows an alternative balance enhancer. Its operation is similar to that of the circuit shown in Figure 3.9. The circuit exhibits high-pass characteristics globally, and a notch is formed by the series resonance induced by L_p and C_s. Different values can be set for the left C_p and right C_p to form two notches of different frequencies.

Figure 3.13 shows the transmission characteristics of the circuit in the differential and common modes. Here, the left C_p and right C_p are set to be equal, and L_p=4.77 nH, C_p=8.49 pF, and C_s=8.49 pF. They behave similarly to those shown in Figure 3.10.

However, owing to the intrinsic high-pass nature of this circuit, the common-mode rejection becomes worse at high frequencies.

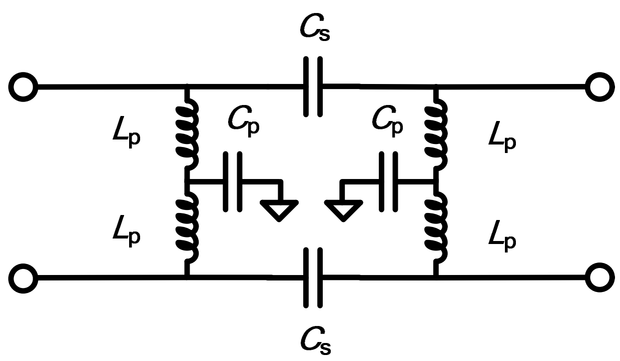

Figure 3.12 High-pass-type balance enhancer

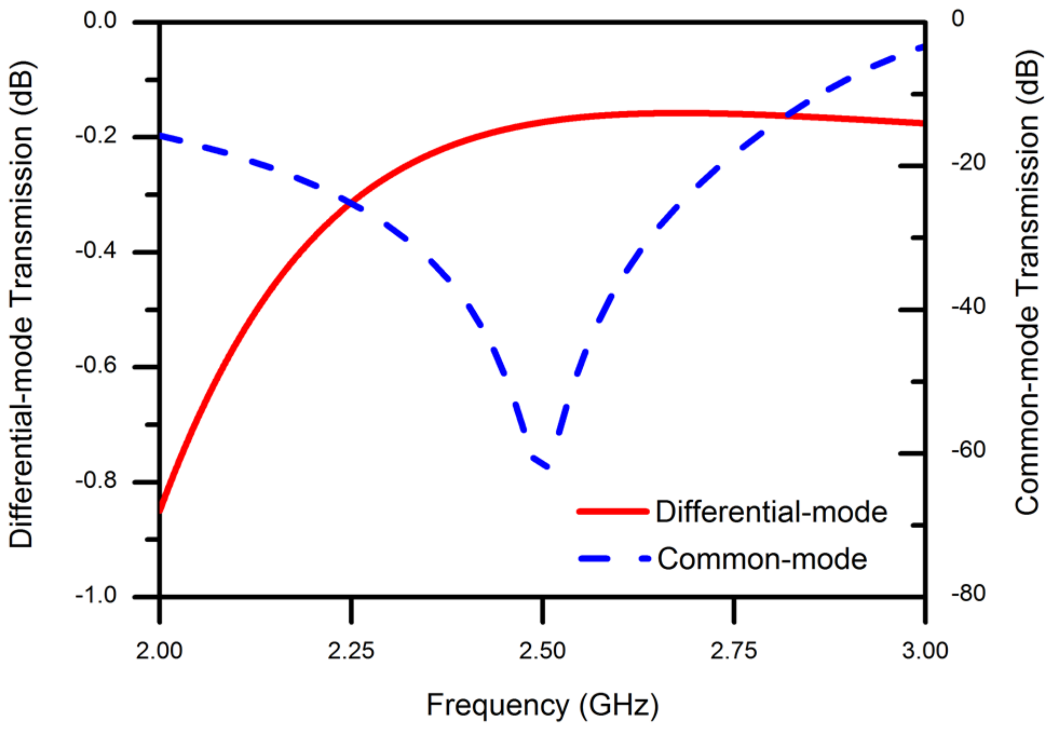

Figure 3.13 Transmission characteristics of high-pass balance enhancer in differential mode and common mode

Figure 3.14 shows the transmission characteristics when the circuit is inserted in the filter topology as shown in the inset. Again, the filter response close to the original design can be achieved owing to the improved common-mode rejection. The intrinsic high-pass characteristic of the enhancer does not significantly affect the total performance, and moderate out-of-band rejection is achieved.

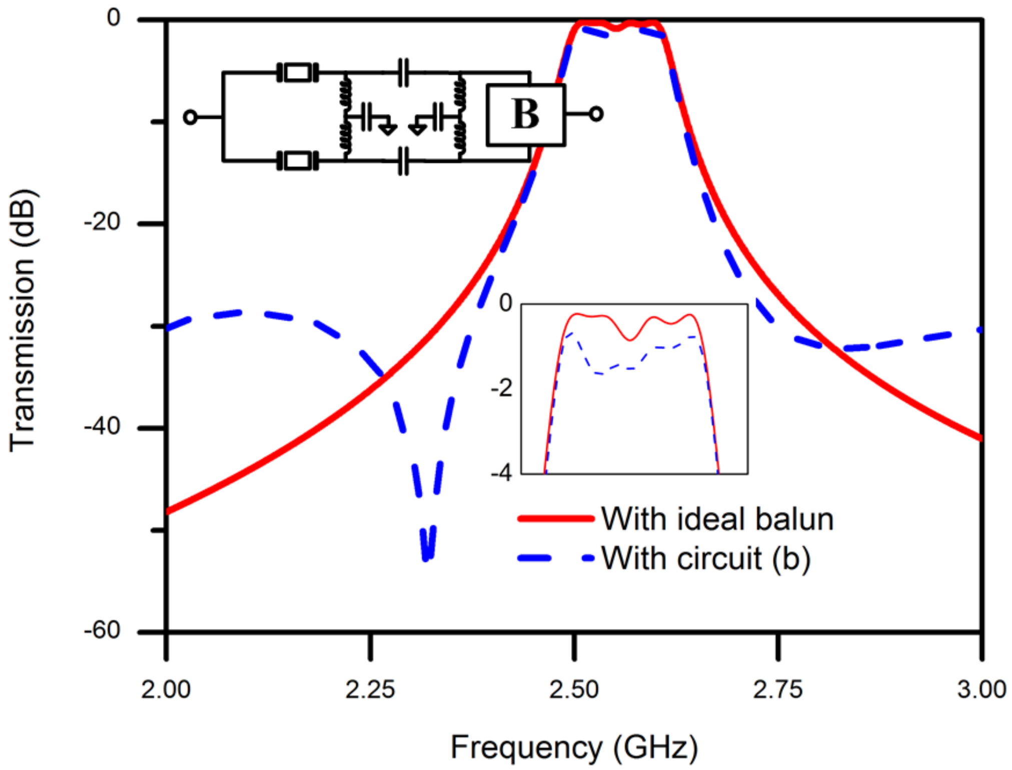

Figure 3.14 Performance of filter with high-pass balance enhancer and commercial balun from MURATA

Note that the out-of-band rejection significantly changes with not only the balun performance but also the setting of the enhancer. For example, the out-of-band rejection above the passband can be improved by reducing the center frequency of the filter and enhancer in the trade off with the rejection level below the passband.

To consider the impact of different balun, use of another commercial balun FI168T155021-T [3.6] from Taiyo Yuden CO., LTD is investigated. Its impedance is 50 and 75 Ω for the unbalanced and two balanced ports, respectively. It has a wide passband of 900-2200 MHz and its minimum insertion loss is 2.3 dB which is much larger than the MURATA one. Figure 3.15 shows the transmission characteristics, which was supplied in the touchstone format from Taiyo Yuden CO., LTD. Comparing with the MURATA one, its S_{21} and S_{31} are much flatter which means it exhibits balun function in much wider range.

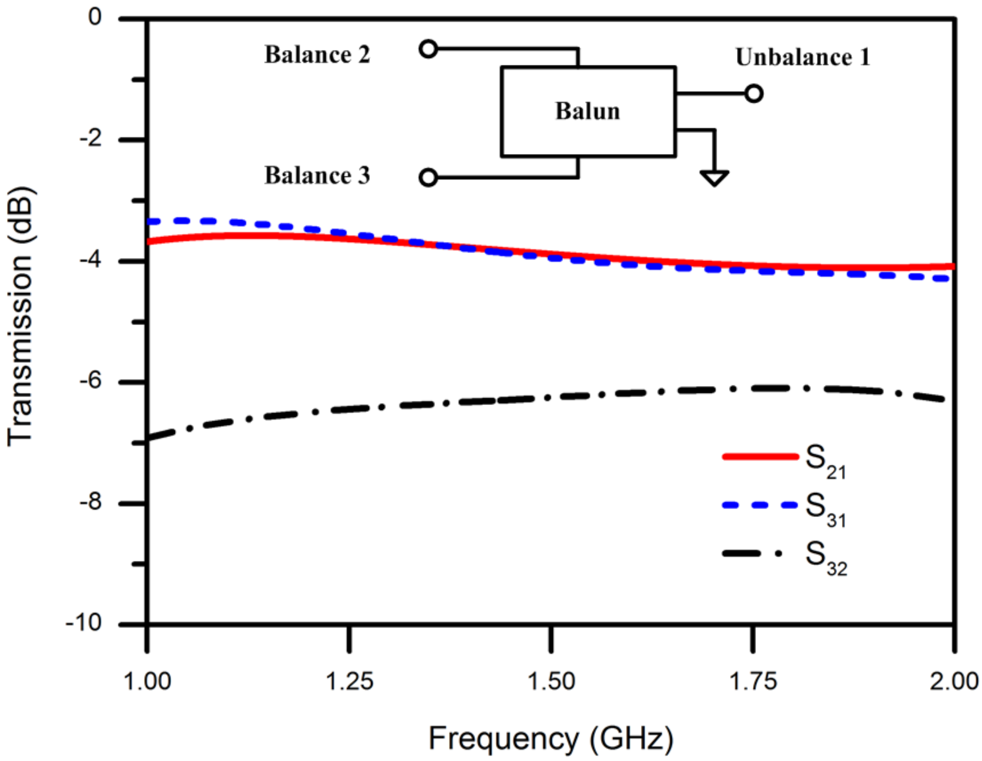

Figure 3.15 Transmission characteristic of the commercial balun from Taiyo Yuden

Figure 3.16 shows the filter characteristic with this balun. In the figure, the simulated result using the ideal balun is also shown. Comparing with the MURATA one, this balun imperfection causes not so serious deterioration in the filter characteristic for its wide passband.

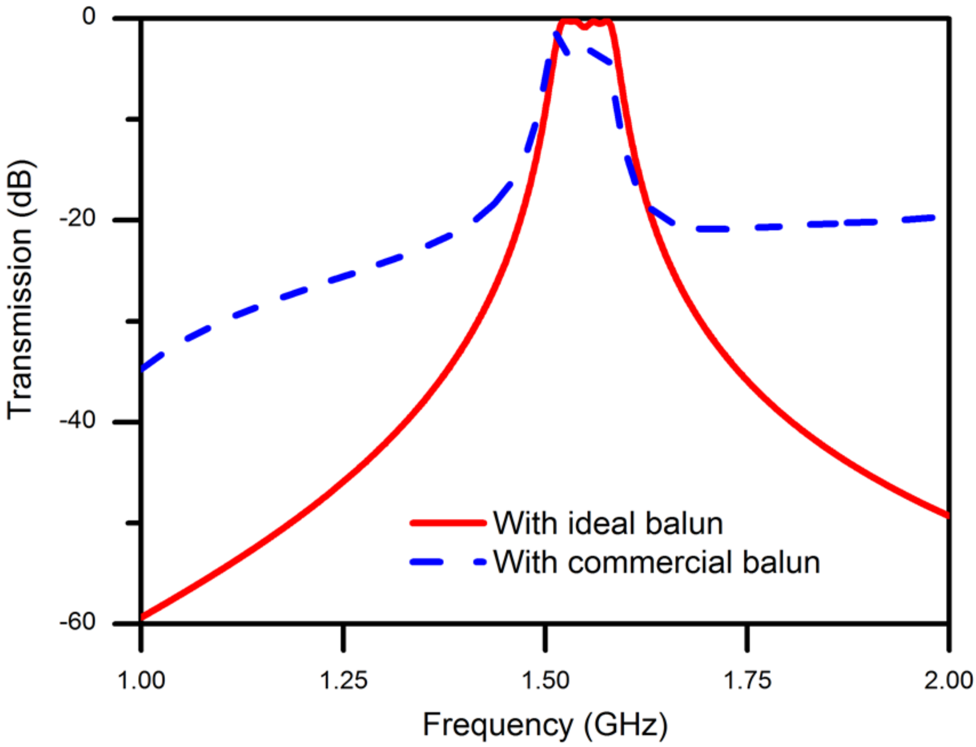

Figure 3.16 Performance of the designed multimode filter with the commercial balun from Taiyo Yuden

Figure 3.17 shows the transmission characteristic when the enhance circuit is inserted in the filter topology as shown in the inset. Comparing with MURATA one, its out-of-band rejection is better especially for the frequencies higher than the passband. It contributes to the flat passband of this balun. The passband is narrower because the center frequency is half of the MURATA one. It is seen that its passband is flat and the average insertion loss is around 1.8 dB. The comparing shows that the filter performance is strongly related to the balun performance.

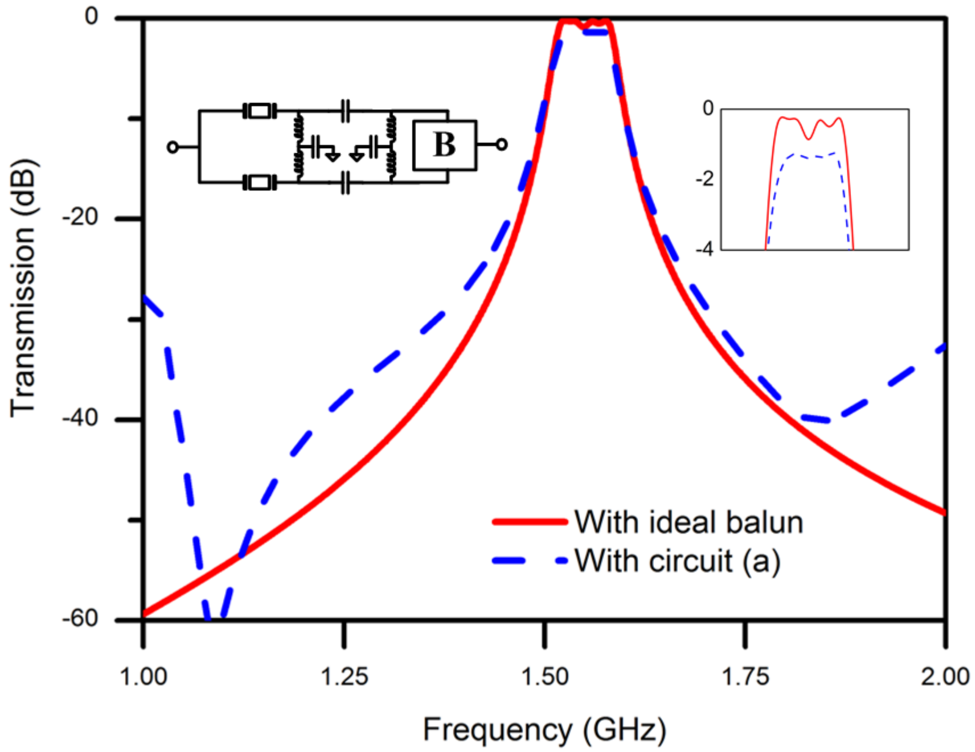

Figure 3.17 Filter performance using low-pass balance enhancer and commercial balun from Taiyo Yuden

3.5 Conclusion

This chapter discussed possibility of realizing multimode filters composed of multiple single-mode resonators by using RF SAW/BAW technologies.

First, the filter operation and design principle were given. It was demonstrated that excellent filter characteristics are achievable by combining multiple single-mode resonators with identical γ values provided that their resonance frequencies and clamped capacitances are set properly.

Next, it was shown that balun imperfection significantly deteriorates the total device performance. Then, two circuits were proposed to improve the common-mode rejection, and their effectiveness was demonstrated.

Reference

[3.1] K. Hashimoto, “5.2 Spurious Responses”, *Surface Acoustic Wave Devices in Telecommunications* (Springer Verlag, 2000) p. 130

[3.2] K. Hashimoto, “5.4.2 Lattice Type Filters”, *Surface Acoustic Wave Devices in Telecommunications* (Springer Verlag, 2000) p. 152

[3.3] S. Beaudin, S. Damphousse, and T. Cameron, “Shoulder Suppressing Technique for dual mode SAW resonators,” *Ultrasonics Symp.,* (1999) p. 389.

[3.4] Datasheet, Murata Manufacturing Co., Balun with part number: LDM0Q2G5010BE005.

[3.5] http://qucs.sourceforge.net/

[3.6] Datasheet, Taiyo Yuden Co., Balun with part number: FI168T155021-T.

4 Conclusions and outlooks

4.1 Conclusions

To obtain high performance, small size and low cost SAW/BAW filters, the following two filters, band reject filter embedded in impedance converter and multi-mode filter with electrically coupled one port resonators were investigated. The results can be concluded as the following,

In chapter 2, the design rule of band reject filter was discussed in detail and verified by fabrication and simulation. When two notches caused by the one port resonators were placed in proximity, two synergy effects occurred: (i) an extra matching point appeared on one side of the transition band. It made the insertion loss at the point smaller and the transition band steeper, and (ii) the dip level became deeper, and the total rejection level improved.

In chapter 3, the design rule of multi-mode filter was discussed. Balun was applied to couple multi-mode resonators. The electrical coupling allowed applying both SAW and BAW one port resonators and good out-of-band rejection could be achieved contributing to the differential structure. Then, it was shown that commercial balun had great influence to the filter performance and additional balance enhance circuit was applied. With the balance enhance circuit, filter could response close to the original design.

4.2 Outlooks

This thesis aims to research the theoretical characteristics of the band reject filter and multimode filter. For this reason, the band reject filter in chapter 2 is not fabricated in whole device but resonators instead. Then, circuit simulator is applied to evaluate the filter with the measured resonators data. Because the key element is based on measured data from practical device, this strategy is efficient to reduce the fabrication process while keeping enough reliability of simulation result. For the same reason, the multimode filter in chapter 3 applies the commercial balun.

In the future, if necessary, the whole filter device could be fabricated and the influence of connection between each circuit element could be evaluated and the power durability and reliability of the whole device could be measured.

Lists of publications

Journals papers

1. **Y. Huang**, J. Bao, G. Tang, Q. Zhang, T. Omori, and K. Hashimoto, "Design Consideration of SAW/BAW Band Reject Filters Embedded in Impedance Converter", *IEEE Trans. Ultrason., Ferroelect., Freq. Control*, 64, (2017) p. 1368.
2. **Y. Huang**, J. Bao, G. Tang, Y. Wang, T. Omori, and K. Hashimoto, "Multimode filter composed of single-mode surface acoustic wave/bulk acoustic wave resonators", *Jpn. J. Appl. Phys*. 56 (2017) 07JD10.
3. **Y. Huang**, J. Bao, X. Li, B. Zhang, G. Tang, T. Omori, and K. Hashimoto, "Influence of Coupling between Rayleigh and SH SAWs on Rotated Y-cut $LiNbO_3$ to Their Propagations", *IEEE Trans. Ultrason., Ferroelect., Freq. Control*, (2018), DOI: 10.1109/TUFFC.2018.2832174.
4. **Y. Huang**, J. Bao, X. Li, B. Zhang, T. Omori, and K. Hashimoto, "Parameter extraction of coupling-of-modes equations including coupling between two surface acoustic waves on SiO_2/Cu/$LiNbO_3$ structures," *Jpn. J. Appl. Phys*. 57 (2018) 07LD13.
5. B. Zhang, T. Han, G. Tang, X. Li, **Y. Huang**, T. Omori, and K. Hashimoto, "Impact of Coupling between Multiple SAW Modes on Piston Mode Operation of SAW Resonators," *IEEE Trans. Ultrason., Ferroelect., Freq. Control* 65, (2018) p. 1062.
6. B. Zhang, T. Han, X. Li, **Y. Huang**, T. Omori, and K. Hashimoto, "Model Parameter Extraction of Lateral Propagating Surface Acoustic Waves with

Coupling on SiO_2/grating/$LiNbO_3$ Structure" *Jpn. J. Appl. Phys*. 57 (2018) 07LD04.

7. X. Li, J. Bao, **Y. Huang**, B. Zhang, T. Omori, and K. Hashimoto, "Application of hierarchical cascading technique to finite element method simulation in bulk acoustic wave devices," *Jpn. J. Appl. Phys*. 57 (2018) 07LC08.
8. X. Li, J.Bao, **Y. Huang**, B. Zhang, G. Tang, T. Omori, and K. Hashimoto, "Use of double-raised-border structure for quality factor enhancement of type II piston mode FBAR." *Microsystem Technologies*, 24 (2018) p.2991.

Conferences papers

1. **Y. Huang**, J. Bao, G. Tang, T. Aonuma, Q. Zhang, T. Omori, and K. Hashimoto, "SAW/BAW band reject filters embedded in impedance converter", *Proc. IEEE Ultrason. Symp.* (2016) DOI: 10.1109/ULTSYM.2016.7728411.
2. **Y. Huang**, J. Bao, G. Tang, Y. Wang, T. Omori, and K. Hashimoto, "Multimode filter composed of single-mode SAW/BAW resonators," *Proc. 37th Symp. Ultrasonics Electronics*, (2016) 1E4-2.
3. **Y. Huang**, J. Bao, X. Li, B. Zhang, G. Tang, T. Omori, and K. Hashimoto, "Influence of coupling between Rayleigh and SH SAWs on rotated Y-cut $LiNbO_3$ to their electromechanical coupling factor," *Proc. IEEE Ultrason. Symp.* (2017) DOI: 11.1109/ULTSYM.2017.8092561.
4. **Y. Huang**, J. Bao, X. Li, B. Zhang, T. Omori, and K. Hashimoto, "Parameter extraction of COM equations including two SAW coupling for TC-SAW structures,"

Proc. 38th Symp. Ultrasonics Electronics, (2017) 1P3-4.

5. **Y. Huang**, J. Bao, G. Tang, T. Aonuma, T. Omori, and K. Hashimoto, "SAW/BAW Band Reject Filters Embedded in Impedance Converter", 日本学術振興会弾性波素子技術第150委員会第144回研究会, (2016) p. 13
6. **Y. Huang**, J. Bao, G. Tang, T. Omori, and K. Hashimoto, "Multi-Mode Filter Composed of Single-mode Surface Acoustic Wave/Bulk Acoustic wave (SAW/BAW) Resonators", 圧電材料・デバイスシンポジウム, (2017) p. 39
7. B. Zhang, T. Han, G. Tang, X. Li, **Y. Huang**, T. Omori, and K. Hashimoto, "Impact of coupling between multiple SAW modes on piston mode operation of SAW resonators," *Proc. IEEE Ultrason. Symp.* (2017) DOI: 10.1109/ULTSYM.2017.8092109.
8. B. Zhang, T. Han, G. Tang, X. Li, **Y. Huang**, T. Omori, and K. Hashimoto, "Model parameter extraction of lateral propagating SAWs with mode coupling on TC-SAW resonators," *Proc. 38th Symp. Ultrasonics Electronics*, (2017) 1P3-3.
9. Q. Zhang, T. Han, B. Zhang, G. Tang, **Y. Huang**, T. Omori, and K. Hashimoto, "Frequency domain FEM analysis of reflector scattering characteristics for SAW tags," *Proc. IEEE Ultrason. Symp.* (2016) DOI: 10.1109/ULTSYM.2016.7728495.
10. X. Li, J. Bao, **Y. Huang**, B, Zhang, T. Omori, and K. Hashimoto, "Traveling wave excitation for FEM simulation of RF SAW/BAW devices," *Proc. IEEE Ultrason. Symp.* (2017) DOI: 10.1109/ULTSYM.2017.8092845.
11. X. Li, J. Bao, **Y. Huang**, B. Zhang, G. Tang, T. Omori, and K. Hashimoto, "Use of

double-raised-border structure for quality factor enhancement of type II piston mode FBAR," *2017 Joint Conference of the European Frequency and Time Forum and IEEE International Frequency Control Symposium*, (2017) DOI: 10.1109/FCS.2017.8088953.

12. X. Li, J. Bao, **Y. Huang**, B, Zhang, T. Omori, and K. Hashimoto, "Application of hierarchical cascading technique to FEM simulation in BAW devices," *Proc. 38th Symp. Ultrasonics Electronics*, (2017) 2E2-2.